Article:
Janpum, C., Pandhal, J. orcid.org/0000-0002-0316-8031, Pombubpa, N. et al. (4 more authors) (2025) Bio-hydrogel formulation for co-immobilization of microalgae and bacteria in living biofilters for nutrient recovery from secondary industrial effluents. Cleaner Engineering and Technology, 29. 101075. ISSN: 2666-7908

https://doi.org/10.1016/j.clet.2025.101075

Cleaner Engineering and Technology 29 (2025) 101075

Contents lists available at ScienceDirect

Cleaner Engineering and Technology

journal homepage: www.sciencedirect.com/journal/cleaner-engineering-and-technology

Bio-hydrogel formulation for co-immobilization of microalgae and bacteria in living biofilters for nutrient recovery from secondary industrial effluents

Chalampol Janpum [a], Jagroop Pandhal [b], Nuttapon Pombubpa [c], Tanakit Komkhum [a], Chonnikarn Sirichan [e], Piyakorn Srichuen [e], Pichaya In-na [a,d,*]

[a] Department of Chemical Technology, Faculty of Science, Chulalongkorn University, Bangkok, 10330, Thailand
[b] Department of Chemical and Biological Engineering, The University of Sheffield, Sheffield, S1 3JD, United Kingdom
[c] Department of Microbiology, Faculty of Science, Chulalongkorn University, Bangkok, 10330, Thailand
[d] Research Unit on Sustainable Algal Cultivation and Applications (RU SACAS), Faculty of Engineering, Chulalongkorn University, Bangkok, 10330, Thailand
[e] Patum Vegetable Oil Co., Ltd., Pathum Thani, 12140, Thailand

ARTICLE INFO

Keywords:
Wastewater treatment
Nutrient recovery
Hydrogel formulation
Biofilters
Co-immobilization

ABSTRACT

The increasing discharge of nutrient-rich industrial effluents poses a significant environmental challenge, necessitating efficient and sustainable wastewater treatment strategies. This study developed a living hydrogel-based biofilter incorporating co-immobilized *Chlorella* sp. and *Bacillus subtilis* TISTR 1415 to enhance nutrient recovery from secondary industrial effluent from vegetable oil factories. Hydrogels were formulated using guar gum and carrageenan, crosslinked with potassium chloride (KCl), and evaluated for their stability and microbial immobilization efficiency. Among the tested formulations, the hydrogel with 0.3 M KCl exhibited optimal properties, including moderate swelling capacity (~1,005 % or ~10 $g_{water}/g_{dry\ hydrogel}$), reduced solubility (~40 %), and enhanced mechanical stability and crosslinking density, leading to improved porosity and microbial retention. These physicochemical properties facilitated efficient nutrient diffusion and sustained cell viability within the hydrogel matrix. The synthetic co-culture biofilter with a 3:1 ratio of *Chlorella* sp. to *B. subtilis* significantly enhanced nutrient removal efficiencies compared to monocultures, achieving 98.68 % ammonium (NH_4^+), 53.45 % phosphate (PO_4^{3-}), and 68.60 % COD removal over 7-day trials. The synergistic interaction between microalgae and bacteria facilitated improved nutrient uptake, organic matter degradation, and enhanced effluent treatment performance. Furthermore, pH and dissolved oxygen levels were significantly influenced by microbial activity, with microalgae contributing to oxygen production and pH elevation, while bacteria aided organic matter breakdown. The living hydrogel-based biofilter presents a promising alternative to conventional wastewater treatment methods by harnessing the synergistic interactions between biological processes and hydrogel immobilization technology. This approach enhances effluent quality and contributes to innovative solutions for environmental protection and nutrient recovery.

1. Introduction

The escalating global demand for industrial production necessitates effective wastewater management strategies. Industrial activities generate substantial volumes of wastewater, containing diverse compositions and potentially harmful pollutants (Oladimeji et al., 2024). Industrial processes generate variable and often complex wastewater streams, posing a significant threat to both aquatic ecosystems and human well-being (Oladimeji et al., 2024). These wastewater effluents often contain a complex mixture of organic and inorganic pollutants, varying widely depending on industrial sources. For example, textile wastewater contains high concentrations of dyes, heavy metals and organic chemicals (Wang et al., 2022), whereas food processing wastewater is rich in organic matter leading to high biological oxygen demand (BOD) and chemical oxygen demand (COD) (Xu et al., 2024a). In addition to organic pollutants, vegetable oil processing wastewater is rich in nutrients, particularly nitrogen (N) and phosphorus (P) (Hartal et al., 2024). The presence of these nutrients in the effluent can lead to serious environmental issues, such as eutrophication of receiving water bodies (Hartal et al., 2024). Effective treatment methods are necessary

* Corresponding author. Department of Chemical Technology, Faculty of Science, Chulalongkorn University, Bangkok, 10330, Thailand.
E-mail address: pichaya.i@chula.ac.th (P. In-na).

https://doi.org/10.1016/j.clet.2025.101075
Received 8 June 2025; Received in revised form 30 July 2025; Accepted 7 September 2025
Available online 10 September 2025

to remove these nutrients before discharge.

Conventional wastewater treatment methods such as activated sludge processes, anaerobic digestion, and membrane filtration, while widely employed, often fall short of providing complete and sustainable solutions (Shamshad and Rehman, 2025). These technologies can be energy-intensive, require extensive land use, generate significant sludge volumes necessitating further treatment and disposal, and may prove ineffective against complex pollutant mixtures (Shamshad and Rehman, 2025). Furthermore, many conventional methods do not actively recover and convert valuable resources that may be present in the wastewater stream. This has stimulated the search for more efficient, cost-effective, and environmentally benign approaches that minimize waste and maximize resource recovery. Bioremediation, utilizing biological systems to degrade or remove pollutants, offers a sustainable alternative to conventional wastewater treatment methods (Srimongkol et al., 2022).

The application of microalgae in wastewater treatment has gained significant traction in recent years, driven by their remarkable capacity for nutrient uptake and converting those nutrients into valuable products (Li et al., 2019). Various microalgal species, including *Chlorella* sp., *Scenedesmus* sp., *Oscillatoria* sp., and *Spirulina* sp. etc., have demonstrated effective removal of N and P from wastewater (Li et al., 2019). Especially, *Chlorella* sp. is a genus of green microalgae renowned for its high nutrient removal capacity, fast growth rate, and high tolerance to various environmental conditions, making it highly suitable for wastewater treatment applications (Adhithya et al., 2025). Species such as *Chlorella vulgaris*, *Chlorella pyrenoidosa*, and *Chlorella sorokiniana* have been widely studied for their ability to absorb N, P, and organic pollutants efficiently, thereby improving water quality (Adhithya et al., 2025). Additionally, their biomass can be harvested for value-added products like biofuels, animal feed, and biofertilizers, offering economic benefits alongside environmental remediation (Li et al., 2019).

In addition, the integration of plant growth-promoting bacteria (PGPB), such as *Bacillus* sp., *Pseudomonas* sp., and *Azospirillum* sp. etc., enhances the efficiency of the bioremediation process by degrading complex organic compounds in wastewater, thereby increasing nutrient bioavailability for microalgal uptake and accelerating the overall treatment process (Guo et al., 2021; Trejo et al., 2012; Yusuf et al., 2013). For example, *Bacillus subtilis* has emerged as a highly effective microbial agent for wastewater treatment due to its robust enzymatic activity and resilience in diverse environmental conditions (Wang et al., 2025). It contributes to the degradation of organic pollutants, including complex carbohydrates, proteins, and lipids, thereby significantly reducing COD levels in effluents (Wang et al., 2025). Additionally, *B. subtilis* has shown potential in reducing ammonium content through simultaneous nitrification and denitrification processes (Wang et al., 2025). These multifaceted mechanisms make bacteria not only valuable for enhancing nutrient removal in integrated co-culture systems but also for contributing to broader environmental safety and sustainability goals. This synergistic interplay between specific microalgal strains and PGPB species offers a promising pathway for significantly improving wastewater treatment efficacy (Sial et al., 2021).

The synergistic interaction between microalgae and bacteria can further enhance the efficiency of biological wastewater treatment. Many studies have demonstrated the beneficial effects of combining microalgae and bacteria in co-cultures for nutrient removal and biomass production (Janpum et al., 2022; Li et al., 2024). Bacteria contribute to nutrient cycling and organic matter degradation by releasing enzymes that break down complex organic matter into simpler nutrients, creating a favorable environment for microalgal growth (Janpum et al., 2022; Li et al., 2024). Conversely, microalgae produce oxygen, which is essential for the aerobic respiration of bacteria, and the combined effects of oxygen production and nutrient byproduct utilization create a synergistic interaction that enhances the overall system efficiency (Janpum et al., 2022; Li et al., 2024). Two primary co-cultivation methods exist: suspension and immobilization systems. Suspension systems are commonly utilized, which maintain microorganisms freely suspended in wastewater, offering simplicity in design and operation and high surface area for pollutant interaction (Caldwell et al., 2021; Janpum et al., 2022). However, they are prone to significant cell washout, high risk of contamination, and high energy requirements for biomass harvesting (Janpum et al., 2022). In contrast, immobilization systems attach or entrap microorganisms within a solid support matrix, offering advantages such as increased cell density, enhanced treatment efficiency, protecting cells from undesirable microorganisms, and reduced washout (Caldwell et al., 2021; Janpum et al., 2022).

Biocomposite or biofilter technology provides a sustainable and efficient approach to wastewater treatment by utilizing immobilized microorganisms (Janpum et al., 2022; Odibo et al., 2024). This method employs an immobilization technique where microorganisms are embedded within a binder or hydrogel matrix, which is then adhered to a support material. Odibo et al. (2024) conducted a comparative study between immobilized and suspended microbial systems, finding that immobilization significantly enhanced treatment efficiency. However, their binder formulation lacked optimization, leading to insufficient durability during wastewater treatment applications. This highlights the necessity for further refinement of hydrogel materials to improve mechanical strength and longevity under operational conditions. The binder or hydrogel matrix, often a natural or synthetic polymer, optimizes pollutant removal and prevents cell washout (Bouabidi et al., 2019). This approach offers a robust and potentially cost-effective solution for advanced wastewater treatment. Realizing the full potential of this biological approach requires careful optimization of the cultivation environment and the immobilization of these microorganisms within a suitable binder matrix.

Hydrogels, three-dimensional polymeric networks capable of absorbing substantial amounts of water, provide an ideal scaffold for microbial growth and activity in bioremediation applications (Van Tran et al., 2018). Their porous structure significantly increases the surface area for microbial interaction with wastewater, enhancing nutrient adsorption and pollutant removal, while immobilization within a hydrogel matrix further improves system stability by retaining biomass (Bouabidi et al., 2019). A wide variety of biopolymers, each offering unique properties, can be used to create these hydrogels, including alginate (a biocompatible polysaccharide from brown seaweeds with excellent gelation properties), cellulose (a renewable, biodegradable polysaccharide from plant cell walls, notable for its mechanical strength and ability to form hydrogels), guar gum (a galactomannan polysaccharide from guar beans with high viscosity and water retention), and carrageenan (a sulfated polysaccharide from red seaweed known for its gelling properties and biocompatibility) (Wong, 2018). The selection of the appropriate biopolymer and the optimization of the hydrogel formulation are crucial for maximizing biofilter performance, with biocompatibility, mechanical strength, porosity, and cost-effectiveness all playing significant roles (Rando et al., 2024).

Guar gum-based hydrogels, in particular, have been attracting considerable attention not only for their effective pollutant adsorption and structural properties, but also for their versatility as biopolymers in biological systems and bioremediation techniques. Their inherent biocompatibility and biodegradability make them suitable for applications ranging from pollutant adsorption to tissue scaffolding and microbial encapsulation. For example, Caldera-Villalobos et al. (2021) and (2022) developed composite hydrogels based on collagen/guar gum incorporated with metal-organic frameworks (MOFs), demonstrating high efficiency in water pollutant removal while also optimizing their biocompatibility for potential applications in both bioremediation and tissue engineering. Furthermore, semi-interpenetrating polymer networks (semi-IPNs) formed from collagen and guar gum have demonstrated significant potential in both biomedical and wastewater treatment applications (Lopez Martinez et al., 2022a; Lopéz Martínez et al., 2022b). Notably, carboxymethylated guar gum hydrogels have shown enhanced dye adsorption performance, further supporting their

suitability for environmental remediation (Yousry et al., 2025).

Moreover, carrageenan, a sulfated polysaccharide extracted primarily from red seaweeds, has been extensively recognized for its unique physicochemical properties contributing to hydrogel formation (Mirzaei et al., 2023). The presence of sulfate ester groups facilitates ionic cross-linking, enhancing gel strength and structural integrity, making it suitable for applications in pollutant adsorption and controlled release systems (Mirzaei et al., 2023). Furthermore, carrageenan hydrogels have demonstrated effective removal of contaminants from pharmaceutical wastewater, highlighting their potential in environmental remediation applications (Afzaal et al., 2024). Its biocompatibility and biodegradability make it suitable for applications ranging from environmental remediation to drug delivery (Sayed et al., 2023). Additionally, the mechanical resilience of carrageenan-based hydrogels under varied environmental conditions justifies their selection in pollutant adsorption technologies (Aboelkhir et al., 2024). These studies and properties collectively emphasize the eco-friendly, biocompatible, and tunable nature of guar gum and carrageenan for applications in sustainable wastewater remediation. Despite the advances in wastewater treatment using microalgae and bacteria using hydrogels, challenges persist, particularly in balancing the hydrogels with desired properties such as strength, cell viability, and nutrient/water uptake.

Further research is needed to optimize hydrogel formulations tailored to specific industrial wastewater characteristics and to determine optimal co-culture ratios of microalgae and bacteria. The ratio of these microorganisms is a critical factor that directly influences the efficiency of nutrient uptake, organic matter degradation, and system stability (Nagabalaji et al., 2023). An imbalanced ratio may lead to competition for resources, which can compromise treatment performance and biomass productivity. Optimizing the co-culture ratio ensures a synergistic relationship, where bacteria degrade complex organic compounds into bioavailable nutrients and microalgae contribute oxygen through photosynthesis (Janpum et al., 2022), enhancing overall biofilter efficiency in the real environment.

This research focuses on developing a novel hydrogel-based living biofilter using co-immobilized *Chlorella* sp. and *Bacillus subtilis* TISTR 1415. The study will thoroughly evaluate suitable hydrogel formulation to achieve an optimized biofilter system for treating real secondary effluent (i.e, tertiary treatment) from the vegetable oil industry, which was selected because it contains high levels of nutrients, particularly N and P, as well as organic matter, which are challenging to remove through conventional treatment processes. The system's performance will be assessed by evaluating nutrient removal efficiencies (N, P, COD), analyzing the impact of varying microalgae-to-bacteria ratios, and quantifying the biofilter's efficiency under real effluent conditions. It is hypothesized that: (1) hydrogel formulations with biological compatibility will enhance microbial viability and activity; (2) co-immobilized consortia at optimized ratios will yield significantly higher nutrient removal than monocultures; and (3) the hydrogel-based biofilter will maintain structural stability and removal efficiency over time, demonstrating its potential as a sustainable tertiary treatment strategy for industrial wastewater.

2. Materials and methods

2.1. Microorganism cultivation

Chlorella sp. (CS), purchased from a local algae farmer in Bangkok, Thailand, was selected for its well-documented ability to efficiently uptake nutrients and tolerate varying wastewater conditions (Adhithya et al., 2025). *Bacillus subtilis* TISTR 1415 (BS), a plant growth-promoting bacterium obtained from the Thailand Institute of Scientific and Technological Research (TISTR), was chosen for its proven capacity to degrade organic pollutants and enhance system stability (Wang et al., 2025). CS was cultivated in 1 L of sterilized Blue-Green medium (BG-11) containing the following concentrations (per liter): $NaNo_3$ 1500 mg, K_2HPO_4 40 mg, $MgSO_4{\cdot}7H_2O$ 75 mg, $CaCl_2{\cdot}2H_2O$ 36 mg, citric acid 6 mg, ferric ammonium citrate 6 mg, $EDTANa_2$ 1 mg, Na_2CO_3 20 mg, H_3BO_3 2.86 mg, $MnCl_2{\cdot}4H_2O$ 1.81 mg, $ZnSO_4{\cdot}7H_2O$ 0.22 mg, $Na_2MoO_4{\cdot}2H_2O$ 0.39 mg, $CuSO_4{\cdot}5H_2O$ 0.08 mg, and $Co(NO_3)_2{\cdot}6H_2O$ 0.05 mg. The culture was contained in a conical flask at 25 ± 2 °C under 2,000 lx illumination (LED white lights) with a 12:12 h light-dark cycle for 14 days, maintaining an air flow rate of 0.1 vvm to enhance growth. BS was initially cultured on nutrient agar plates at 37 °C. For inoculum preparation, a 250 mL culture in nutrient broth liquid medium (beef extract 3 $g{\cdot}L^{-1}$ and peptone 5 $g{\cdot}L^{-1}$) was grown in a 500 mL Erlenmeyer flask on an incubator shaker (200 rpm, 37 °C) for 2 days.

2.2. Hydrogel preparation

Guar gum (GG) and carrageenan (CG), both food-grade (food additive) biopolymers with molecular weights of 535 $g{\cdot}mol^{-1}$ and 788 $g{\cdot}mol^{-1}$, respectively, were purchased from Bangkok Chemical Co., Ltd., Thailand. Hydrogels were prepared using both GG and CG as bio-based binders, and potassium chloride (KCl) as a crosslinking agent. A 15 mM mixture of GG and CG in deionized (DI) water was prepared by dissolving the respective polymers in heat-sterilized DI water (60–70 °C) under continuous stirring with an overhead stirrer at 1200 rpm until a homogeneous mixture was achieved. Different concentrations of KCl solution (0.1, 0.3, 0.5, and 1.0 M) were then added to the GG/CG mixture as crosslinking agents to produce five distinct hydrogel formulations (GG/CG (control hydrogel), GG/CG_0.1KCl, GG/CG_0.3KCl, GG/CG_0.5KCl, and GG/CG_1.0KCl). The mixtures were heated to 80–90 °C to facilitate crosslinking and then cast as thin films in silicone trays. After casting the film, the hydrogel was allowed to set at 25 ± 2 °C and subsequently washed with DI water until a neutral pH was achieved. The films were then allowed to dry completely at 40 ± 2 °C overnight before being used in the subsequent steps (solubility and water uptake tests).

2.3. Living biofilter production and cell immobilization

Living biofilters were constructed using a three-step process. First, cotton fabrics, a natural biodegradable fiber with good biocompatibility, were cut into 8 × 4 cm^2 as a support material, sterilized by autoclaving at 121 °C for 15 min, and then dried at 105 ± 2 °C for 3 h and stored in a silica gel desiccator until use. Second, CS and BS were mixed using a vortex mixer for 1–2 min at various ratios (Table 1), representing monocultures and co-cultures with different proportions (1:0, 0:1, 3:1, 1:1, and 1:3). The mixtures were then harvested by centrifugation at 4,000 rpm for 15 min. Third, the cell pastes (either mono- or co-cultures) were thoroughly mixed with the five hydrogel formulations using an overhead stirrer (as described in Section 2.2) at 250 rpm and 30 ± 2 °C until a homogeneous mixture was obtained. This mixture (15 mL) was then carefully coated onto the prepared cotton fabric and allowed to dry at 25 ± 2 °C, solidifying the hydrogel and immobilizing the cells to produce the living biofilters (See the schematic diagram of biofilters in Fig. 1). This preparation was modified from In-na et al. (2020) and

Table 1
The mixing ratios between microalgae and bacteria.

Culture	Microalgae to bacteria ratios	*Chlorella* sp. (CS) ($\times 10^8$ cell·mL^{-1})	*B. subtilis* (BS) ($\times 10^8$ CFU·mL^{-1})	Named
Monoculture	1:0	1	–	1:0 CS
	0:1	–	1	0:1 BS
Co-culture	3:1	3	1	3:1 CS/BS
	1:1	1	1	1:1 CS/BS
	1:3	1	3	1:3 CS/BS

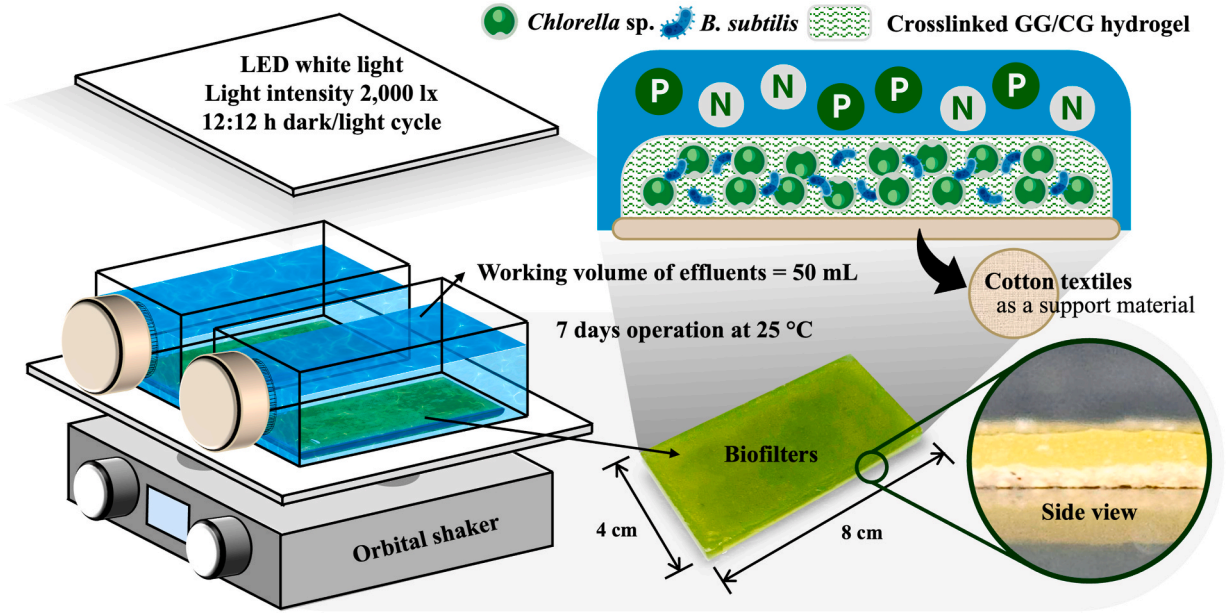

Fig. 1. Schematic diagram of the effluent treatment setup and the guar gum/carrageenan-based biofilter design; N represents nitrogen (as ammonium, NH_4^+) and P represents phosphorus (as phosphate, PO_4^{3-}) present in the effluent.

Odibo et al. (2024).

2.4. Hydrogel characterization

2.4.1. Hydrogel solubility and water uptake tests

Five different hydrogel formulations were prepared and characterized to assess their solubility and water uptake capacity. For the solubility test, the hydrogel films (1.5 × 3 cm^2) were weighed to determine their initial dry weight (W_i). The samples were then immersed in 100 mL of DI water and continuously stirred using a magnetic stirrer at 100 rpm and 25 ± 2 °C for 24 h. Afterward, the insoluble residue was filtered, dried, and weighed to obtain the final dry weight (W_f). The percent solubility was calculated according to equation (1) (Rahman et al., 2021). For the water uptake test, the hydrogel films (3 × 3 cm^2) were weighed to determine their initial dry weight (W_d). The samples were immersed in 50 mL of DI water (without stirring) in a beaker at 25 ± 2 °C. At predetermined time intervals (1, 24, 48, and 72 h), the samples were removed, excess surface water was carefully blotted, and the swollen weight (W_s) was measured. The percentage of water uptake was calculated using equation (2) (Rahman et al., 2021). All measurements were performed in triplicate (n = 3) for each hydrogel formulation.

$$\text{Solubility}\ (\%) = (W_i - W_f) \times 100 \ / \ W_i \quad (1)$$

$$\text{Water uptake}\ (\%) = (W_s - W_d) \times 100 \ / \ W_d \quad (2)$$

2.4.2. Hydrogel adhesion and cytotoxicity tests

This experiment was modified from Komkhum et al. (2025). To assess cell adhesion, biofilter samples (prepared with each hydrogel formulation) were subjected to a cell release assay. Biofilter samples (1 × 1 cm^2) with each hydrogel formulation were tested in triplicate (n = 3) and placed in an individual well of a 12-well plate containing 2 mL of sterilized DI water. The plates were incubated on an orbital shaker at 80 rpm in the dark at 25 ± 2 °C. The DI water was replaced with fresh DI water every 1, 24, 48, and 72 h. At each time point, an aliquot of the supernatant from each well was carefully removed and analyzed for cell density using hemocytometer cell counting. The initial cell density (N_{int}) was determined from the same biofilter preparation before the cell release experiment using the same counting method. The percentage of cell release at each time point was calculated according to equation (3), where R_i represents the number of cells released (cells·mL^{-1}) at a given time point.

The cytotoxicity of the different hydrogel formulations was assessed using a cell viability assay based on optical density (OD) measurements. A mixed cell paste of CS and BS was harvested by centrifugation at 4,000 rpm for 15 min. One milliliter of this cell paste was then added to each well of a 12-well plate, along with 1 mL of each hydrogel formulation (n = 3 replicates per formulation). The plate was incubated at 25 ± 2 °C for 7 days under a 12:12 h light/dark cycle. The OD at 750 nm was measured using a UV–Vis spectrophotometer at the initial (day 0) and final (day 7) of the cytotoxicity test; digital images were also recorded. The percentage of cell viability was calculated according to equation (4), where OD_i and OD_f represent the optical density at the beginning and end of the experiment, respectively, and OD_b represents the optical density of a well containing only the relevant hydrogel formulation (without cells).

$$\text{Cells released}\ (\%) = R_i \times 100 \ / \ N_{int} \quad (3)$$

$$\text{Cell viability}\ (\%) = (OD_f - OD_b) \times 100 \ / \ (OD_i - OD_b) \quad (4)$$

2.4.3. FTIR-ATR and SEM analyses

Fourier Transform Infrared spectroscopy with Attenuated Total Reflectance (FTIR-ATR) analysis was employed to confirm the presence of crosslinking bonds and characterize the functional groups of the five hydrogel formulations (GG/CG, GG/CG_0.1KCl, GG/CG_0.3KCl, GG/CG_0.5KCl, and GG/CG_1.0KCl). FTIR-ATR spectra were acquired using a Nicolet iS5-iD7 (Thermo Scientific, USA), equipped with a diamond crystal ATR accessory. Hydrogel films (1 × 1 cm^2) were dried in a vacuum oven at 60 ± 2 °C under −0.1 MPa and then analyzed. For each formulation, at least three replicate spectra were collected at different locations on the film to ensure representative sampling.

The surface morphology of the samples was examined using a scanning electron microscope (SEM), model JEOL JSM-5410LV, operated in low vacuum mode at an accelerating voltage of 20 kV. Imaging was performed at different magnifications to evaluate surface features, porosity, and structural uniformity. Prior to the SEM analysis, the samples (1 × 1 cm^2), including cotton fabrics coated with GG/CG hydrogels, were prepared using various concentrations of KCl, as well as

biofilter samples in which microorganisms were immobilized within the GG/CG hydrogel matrix on cotton fabrics. Biofilter samples were collected both before and after effluent treatment trails. The dried samples were then mounted on aluminum stubs using carbon adhesive tape and sputter-coated with a thin layer of gold to enhance electrical conductivity and image resolution.

2.5. Decision matrix for suitable condition selectivity

The optimal hydrogel formulation of biofilter production for effluent treatment was determined using a weighted decision matrix (Kosky et al., 2021). Four key parameters were considered, each with a maximum score of 25 points. The first parameter, hydrogel solubility score (V_1), requires hydrogel to be less soluble. The second parameter, water uptake score (V_2), assesses the hydrogel's ability to absorb water at a moderate level between 8 and 10 g of water per gram of dry hydrogel (800–1000 % swelling), as excessive absorption may cause the gel to break easily, while insufficient absorption could hinder nutrient uptake. The third parameter, cell adhesion score (V_3), measures how well cells adhered to the hydrogel matrix, with higher adhesion being preferable. The last parameter, cell viability score (V_4), evaluates the survival rate of cells, where a higher viability value was desired. Each parameter was assigned equal weight (25 %) in the decision matrix, and their respective scores were calculated using equations (5)–(8). The total selective score (maximum 100 points) was calculated as the sum of the weighted scores for each parameter using equation (9). The hydrogel formulation with the highest total score was selected as the optimal formulation for effluent treatment trials.

$$\text{Hydrogel solubility score } (V_1) = \left(100 - X_{s,i}\right) \times 0.25 \tag{5}$$

$$\text{Water uptake score } (V_2) = 25 - \left(\frac{\left|X_{w,i} - \overline{X}_w\right| \times 100}{\left|X_{w,i} - \overline{X}_w\right|_{\max}} \times 0.25\right) \tag{6}$$

$$\text{Cell adhesion score } (V_3) = \left(100 - X_{a,i}\right) \times 0.25 \tag{7}$$

$$\text{Cell viability score } (V_4) = \left(X_{v,i} \times 100 \ / \ X_{v,\max}\right) \times 0.25 \tag{8}$$

$$\text{Total selective score} = \sum_{i=1}^{4} (V_i) \tag{9}$$

Where $X_{s,i}$ is the percentage of solubility for each hydrogel formulation, $X_{w,i}$ is the percentage of water uptake for each hydrogel formulation, $\overline{X}_w$ is the average percentage of water uptake across all hydrogel formulations, $X_{a,i}$ is the percentage of cell released for each hydrogel formulation, $X_{v,i}$ is the percentage of cell viability for each hydrogel formulation, and V_i represents the score for each parameter.

2.6. Effluent treatment tests

Effluent treatment experiments were conducted using secondary effluent from Patum Vegetable Oil Company, Ltd., Pathum Thani, Thailand, which had undergone reverse osmosis treatment at the factory. The effluent, stored at 4 °C in a refrigerator before use, had its initial nutrient composition detailed in Table 2. To ensure that only the introduced microorganisms (CS and BS) contribute to the nutrient removal process and to prevent interference from native microorganisms or pathogens present in the effluent, the effluent was autoclaved before use in the experiment. Living biofilters (8 × 4 cm^2), prepared as described in Section 2.3, containing different ratios of CS and BS, were submerged in 50 mL of autoclaved effluent (working volume) for each experimental run (n = 3) within 120 mL of sealed glass containers. In the experiment, a biofilter without mixed microorganisms served as a control condition. Experiments were conducted under batch conditions in a closed system for 7 days at 25 ± 2 °C, with a 12:12 h light/dark cycle and continuous shaking at 40 rpm on an orbital shaker, with 2000 lx of illumination provided by white light LED panel (Fig. 1). Following the 7-day incubation period, samples were collected to determine the remaining concentrations of ammonium (NH_4^+), phosphate (PO_4^{3-}), and COD, as well as pH and dissolved oxygen (DO) concentration during effluent treatment trials. NH_4^+ and PO_4^{3-} concentrations were determined using the ASTM manual of water and environmental technology D1426-92 (Nessler Method) and standard methods for the examination of water and effluent (Amino Acid Method), respectively, employing HI733 and HI717 Checker®HC (Hanna Instruments, Inc., USA) for analysis. The COD of the effluent samples was determined using a Hanna Instruments HI97106 COD meter, following an adaptation of the US EPA method 410.4 for surface and effluent COD analysis. The pH and DO levels were measured using a portable EC900 AMTAST meter kit (Protronics Co., Ltd., Thailand). Nutrient (NH_4^+ and PO_4^{3-}) and COD removal efficiencies, and nutrient absorption rates, were calculated using equations (10) and (11), where C_i and C_f represent the initial and final concentrations ($mg \cdot L^{-1}$) of the nutrient (NH_4^+ and PO_4^{3-}) or COD, respectively; V is the working effluent volume (L); t is the treatment time (day); and g is the initial biomass dry weight ($g_{biomass}$).

$$\text{Removal efficiency } (\%) = \left(C_i - C_f\right) \times 100 \ / \ C_f \tag{10}$$

$$\text{Nutrient absorption rate } \left(mg \cdot day^{-1} \cdot g_{biomass}^{-1}\right) = \left(C_i - C_f\right) \times V \ / \ t \times g \tag{11}$$

Table 2
Characteristics of the autoclaved secondary effluent.

Composition	Initial concentration
Ammonium (NH_4^+)	7.57 ± 0.25 $mg \cdot L^{-1}$
Phosphate (PO_4^{3-})	386.67 ± 5.77 $mg \cdot L^{-1}$
Total carbon (TC)	28.07 ± 1.16 $mg \cdot L^{-1}$
Inorganic carbon (IC)	22.83 ± 1.32 $mg \cdot L^{-1}$
COD	311.00 ± 6.56 $mg \cdot L^{-1}$
DO	4.55 ± 0.27 $mg \cdot L^{-1}$
pH	7.90 ± 0.03

2.7. Statistical analysis

Statistical analysis was performed using the Real Statistics Resource Pack, an extension for Microsoft Excel. For data exhibiting normal distribution, as confirmed by Shapiro-Wilk tests, one-way analysis of variance (ANOVA) and Tukey's HSD post-hoc test were used to evaluate significant differences among treatment groups. The Kruskal-Wallis test, followed by pairwise Mann-Whitney U tests, was used for non-normally distributed data. Differences were considered statistically significant at $p < 0.05$. Results were expressed as the mean ± standard deviation.

3. Results and discussion

3.1. Characterization of GG/CG hydrogels

3.1.1. Hydrogel solubility

The solubility assessment of hydrogels formulated with GG and CG, crosslinked using varying concentrations of KCl, reveals a clear inverse relationship between KCl concentration and hydrogel solubility (Fig. 2a). The control hydrogel (GG/CG, without KCl) exhibited the highest solubility (71.31 ± 3.78 %), reflecting a less crosslinked and less structurally robust network. The addition of KCl, which acted as a crosslinking agent, significantly decreased the solubility, with values of 48.01 ± 2.67 % (GG/CG_0.1KCl), 39.88 ± 2.33 % (GG/CG_0.3KCl), 35.81 ± 2.39 % (GG/CG_0.5KCl), and 16.47 ± 7.06 % (GG/CG_1.0KCl), (ANOVA: $F(4,10) = 107.57$, $p < 0.05$). The photographs of the hydrogels further support these findings (Fig. 2b). The GG/CG hydrogel appears more dissolved and less structurally intact than the other formulations. As the KCl concentration increases, the hydrogels can

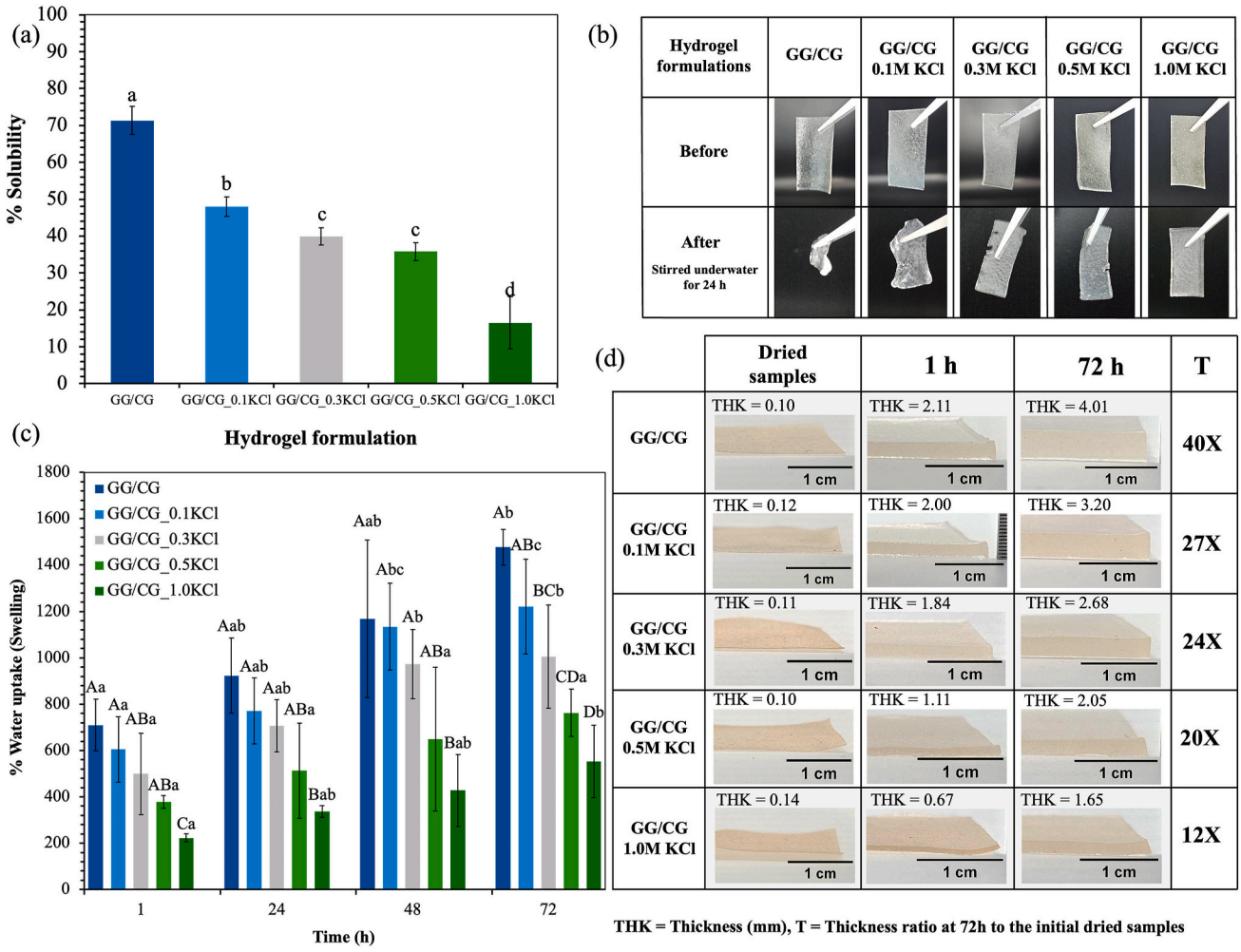

Fig. 2. Hydrogel characterization of GG/CG hydrogels with different KCl concentrations, including (a) The percentage solubility, which differed significantly ($p < 0.05$, ANOVA, Tukey's post hoc test) and are denoted by *different lowercase letters*, (b) photographs of hydrogel characteristics after 1 and 24 h of underwater stirring, (c) the percentage water uptake at various time points over 72 h, which differed significantly ($p < 0.05$, ANOVA, Tukey's post hoc test) and are denoted by *different capital letters*, columns for time points (1, 24, 48, and 72 h), and *lowercase letters*, columns for incubation times (1 vs 24 vs 48 vs 72 h), and (d) photographs of hydrogel swelling characteristics after 1 and 72 h of water immersion.

improve structural integrity, appearing less swollen, more solid, and less prone to disintegration in water. This visual observation was consistent with the solubility data, confirming the successful crosslinking of the hydrogel network by KCl. From a physicochemical perspective (Fig. 4), KCl-induced crosslinking in this study exemplifies ionic physical crosslinking, wherein potassium ions (K^+) electrostatically interact with sulfate groups on the polysaccharide chains of CG (Fig. 4b) (Mirzaei et al., 2023; Rhein-Knudsen et al., 2015). These interactions facilitate the formation of ionic bridges between polymer chains, effectively increasing the density of crosslinking points within the hydrogel matrix (Rhein-Knudsen et al., 2015). The enhanced crosslinking density promotes tighter packing of the biopolymer chains (Fig. 4a), thereby restricting chain mobility and hindering water penetration. Consequently, this structural compaction reduces both the swelling capacity and solubility of the hydrogel in aqueous environments, particularly at higher KCl concentrations (Mirzaei et al., 2023). Similar behavior had been reported in the literature. For example, Lei et al. (2022) investigated the effects of CG and GG on the rheological and microstructural properties of phycocyanin gels and observed that the addition of these polysaccharides reinforces the network structure and reduces sensitivity to deformation. Although their study focused on rheological properties, the underlying mechanism of enhanced crosslinking was analogous to this finding, in which KCl strengthened the network via ionic interactions with CG, thereby reducing solubility (Lei et al., 2022). Furthermore, research work on GG-based hydrogels for agricultural applications has been shown that increased crosslinker (or salt) concentrations reduce swelling capacity and solubility, leading to improved structural integrity—a trend similar to our results. Abdel-Raouf (2019) reviewed GG-based hydrogels and noted that enhanced crosslinking (via chemical or ionic agents) results in lower solubility and better water retention, which can be beneficial for controlled release applications.

3.1.2. *Hydrogel water uptake*

The water uptake data reveal a significant inverse relationship between KCl concentration and the hydrogel's water absorption capacity. The control hydrogel (GG/CG) showed the highest water absorption at all time points (1 h, 24 h, 48 h, and 72 h), reaching 1,477.09 ± 77.70 % after 72 h (Fig. 2c). The addition of KCl, which acted as a crosslinking agent, resulted in a significant decrease in water absorption at all time points, with the water uptake values after 72 h being 1,220.43 ± 204.89 %, 1,005.20 ± 222.73 %, 762.44 ± 101.88 %, and 552.38 ± 156.49 % for the formulations GG/CG_0.1KCl, GG/CG_0.3KCl, GG/CG_0.5KCl, and GG/CG_1.0KCl, (ANOVA: $F_{(4,10)} = 12.76$, $p < 0.05$), respectively. These values showed a progressive decrease in water uptake, indicating that the structure became more compact and less porous with increasing KCl concentration (see Fig. 5). The initial rapid water uptake in the first

hour also reflects this trend, further supporting the hypothesis that KCl crosslinking reduces the hydrogel's ability to swell. Fig. 2d illustrates the significant increase in hydrogel thickness after immersion in water for 72 h compared to the initial state. The numerical data indicated by "T" represent the swelling ratio, calculated as the thickness at 72 h relative to the initial thickness of the dried hydrogel (Fig. 2d). The control hydrogel (GG/CG), which was prepared without KCl crosslinks, exhibited the highest degree of swelling (40X), indicating the presence of a loosely organized and highly porous polymer network with sufficient space to facilitate the easy penetration and retention of water molecules within the gel matrix. This reduction in water absorption is attributed to the increased number of ionic crosslinking points formed via electrostatic interactions between K^+ and the sulfate groups in the polysaccharide chains of CG, which induces matrix contraction (Mirzaei et al., 2023; Rhein-Knudsen et al., 2015). As a result, the polymer network becomes denser and less capable of absorbing and retaining water molecules. As the KCl concentration increased, the hydrogel structure became more compact and the swelling degree decreased, especially the GG/CG_1.0KCl hydrogel displayed the lowest swelling (12X). This trend was consistent with previous reports in the literature. For example, Wu et al. (2009) have demonstrated that a higher crosslinking density leads to a more compact polymer network that restricts chain mobility and limits water diffusion, resulting in lower swelling ratios. Similarly, research on cellulose-based hydrogels has reported that enhanced crosslinking, whether via chemical or ionic means, diminishes the network's porosity and water absorption capacity (Nasution et al., 2022). Moreover, research focusing on CG hydrogels crosslinked with KCl has revealed that while crosslinking enhances mechanical strength, it concurrently reduces water uptake capacity (Markale et al., 2023). This was attributed to the formation of a more compact and less porous structure, which limited the hydrogel's swelling ability (Markale et al., 2023). These findings were consistent with the current experiment, where increasing KCl concentrations led to a denser network and reduced water absorption.

3.1.3. *Hydrogel adhesion*

The cells released assay results reveal a correlation between KCl concentration in the hydrogel and the degree of cell adhesion. The control hydrogel (GG/CG, without KCl) exhibited the highest cells released at all time points (1 h, 24 h, 48 h, and 72 h), reaching 25.64 ± 2.36 % after 72 h (Fig. 3a). Conversely, increasing KCl concentration resulted in a significant decrease in cells released, suggesting enhanced cell adhesion, with hydrogels containing 0.1 M, 0.3 M, 0.5 M, and 1.0 M KCl showing progressively lower cells released percentages (17.95 ± 1.41 %, 13.62 ± 0.97 %, 7.29 ± 1.32 %, and 4.58 ± 1.27 %, respectively, at 72 h), (ANOVA: $F(4,10) = 90.09$, $p < 0.05$), indicating that KCl effectively strengthens cell attachment to the hydrogel matrix. This enhanced cell adhesion was likely attributed to the increased

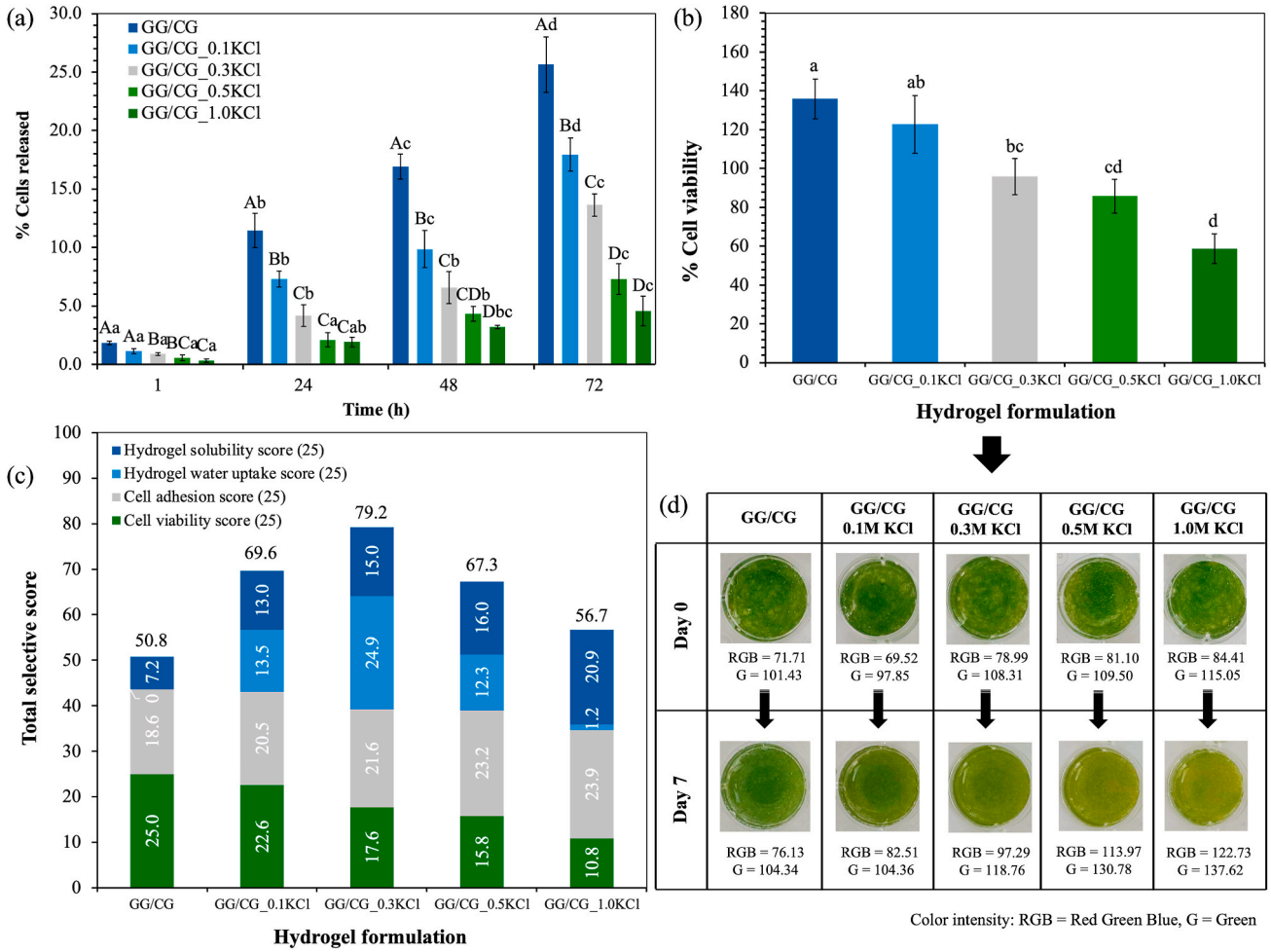

Fig. 3. Evaluation of hydrogel formulations of GG/CG hydrogels with different KCl concentrations for cell immobilization, including (a) the percentage cell released at various time points over 72 h, which differed significantly ($p < 0.05$, ANOVA, Tukey's post hoc test) and are denoted by *different capital letters*, columns for time points (1, 24, 48, and 72 h), and *lowercase letters*, columns for incubation times (1 vs 24 vs 48 vs 72 h), (b) the percentage cell viability after 7 days, which differed significantly ($p < 0.05$, ANOVA, Tukey's post hoc test) and are denoted by *different lowercase letters*, (c) the bar chart of the decision matrix for selecting the optimal hydrogel formulation conditions for effluent treatment, (d) photographs of hydrogel characteristics before (day 0) and after (day 7) cytotoxicity test.

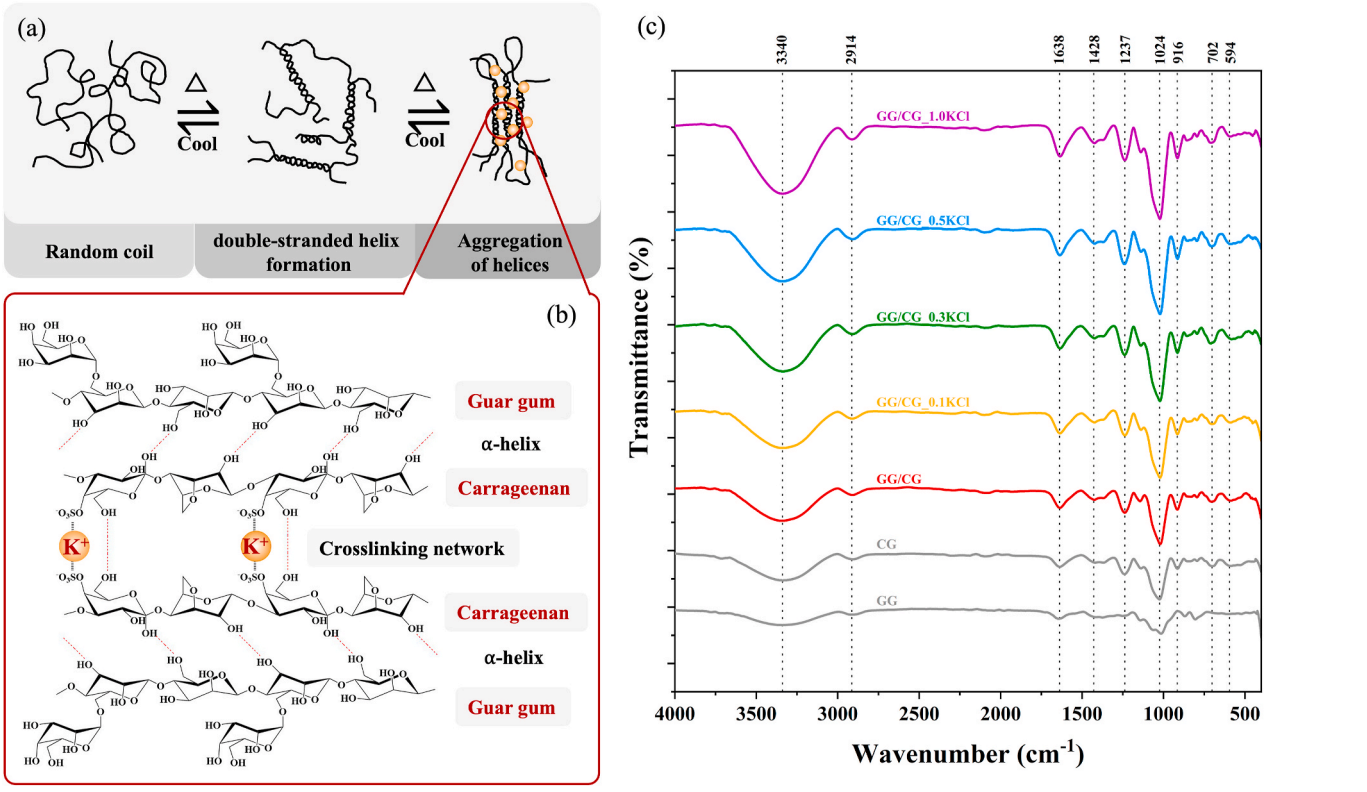

Fig. 4. Mechanism of hydrogel crosslinking and structural analysis, including (a) the schematic stages of the hydrogel crosslinking process and gelation mechanism (reference from (Wong, 2018)), (b) the crosslink mechanism of GG and CG in the presence of K^+ ions (reference from (Rhein-Knudsen et al., 2015)), (c) FTIR spectra of GG, CG, GG/CG, and crosslinked GG/CG with different KCl concentrations.

crosslinking density within the hydrogel network induced by KCl (Ji et al., 2023). The gradual increase in the number of cells released over time (from 1 h to 72 h), observed for all formulations, suggests a time-dependent detachment process. At first, the cell-hydrogel with strong bonds released cells slowly, but over time, more cells were released, possibly because some of the hydrogels were water-soluble, according to the results of hydrogel solubility. The findings suggested that the crosslinked hydrogel played an important role in enhancing cell retention within the hydrogel, which was essential for maintaining the effectiveness and stability of the biofilter (Princen et al., 2023). The increased crosslinking zones reduce the hydrogel's mesh size and alter its porosity (see Fig. 5), creating greater molecular entanglement (Croitoru et al., 2020). These structural changes hinder the diffusion of cells and solutes, slowing the release of encapsulated cells (Croitoru et al., 2020). As a result, the denser network produced at high KCl leads to improved microbial immobilization efficiency and biofilter stability by retaining cells more effectively within the matrix. Our findings were in line with several published studies that demonstrated the pivotal role of crosslinking density in modulating cell–matrix interactions. For instance, Caliari and Burdick (2016) reported that alginate hydrogels crosslinked with cations like calcium have demonstrated improved cell encapsulation and retention due to the formation of stable ionic bridges between polymer chains. Similarly, Nicodemus and Bryant (2008) investigated chitosan-based hydrogels and demonstrated that higher degrees of deacetylation, leading to increased crosslinking, result in slower degradation rates and improved cell adhesion due to enhanced hydrophobic interactions. Additionally, higher crosslinking densities result in smaller mesh sizes within the hydrogel network, potentially hindering cell migration and detachment (Solbu et al., 2023).

3.1.4. Hydrogel cytotoxicity

The bar graphs illustrating the percentage of cell viability in GG/CG hydrogels at varying KCl concentrations are presented in Fig. 3b. The cell viability test results indicated a negative correlation between the KCl concentration in the hydrogels and the viability of the CS/BS co-cultures, which may indicate the possible cell-damaging effect of KCl. The results showed a clear trend of significantly decreased cell viability with increased KCl concentration, (ANOVA: $F(4,10) = 25.63$, $p < 0.05$). The control hydrogel (GG/CG, without KCl) exhibited the highest cell viability (135.91 ± 10.23 %), exceeding 100 %, which indicated that cell growth exceeded the initial inoculum. The GG/CG_0.1KCl formula showed a viability of 122.77 ± 14.81 %, which still indicated growth. However, viability progressively decreased to 95.87 ± 9.20 % (0.3M KCl), 85.79 ± 8.84 % (0.5M KCl), and 58.81 ± 7.62 % (1.0M KCl), indicating an increase in cell death with higher KCl concentrations. The photographs of the hydrogels further support these findings (Fig. 3d). The control hydrogel (GG/CG) showed the highest green color intensity on day 7 (RGB = 76.13), which aligned with the highest cell viability percentage (135.91 ± 10.23 %). The color intensity remained relatively high in the GG/CG_0.1KCl formulation (RGB = 82.51), which was consistent with the high cell viability (122.77 ± 14.81 %). In contrast, as the KCl concentration increased, the green color intensity decreased significantly (RGB = 97.27 for GG/CG_0.3KCl, RGB = 113.97 for GG/CG_0.5KCl, and RGB = 122.73 for GG/CG_1.0KCl), which possibly indicated a reduction in cell density and correlated with the decreased percentage of viability observed in the cell viability assay. The observed decrease in green color with increasing KCl concentration provided visual confirmation of the cytotoxic effects of KCl on the CS/BS co-culture, reinforcing the conclusions drawn from the OD-based cell viability assay. The observed increase in cytotoxicity at higher KCl concentrations may be attributed to reduced matrix porosity from enhanced ionic physical crosslinking, which may restrict nutrient transport to encapsulated cells, reduce their metabolic activity, and influence cell viability (Guan et al., 2017). This restricted diffusion can lower cellular metabolic activity and viability, emphasizing that high crosslinking density affects the biocompatibility of the hydrogels (Guan et al., 2017). The observed

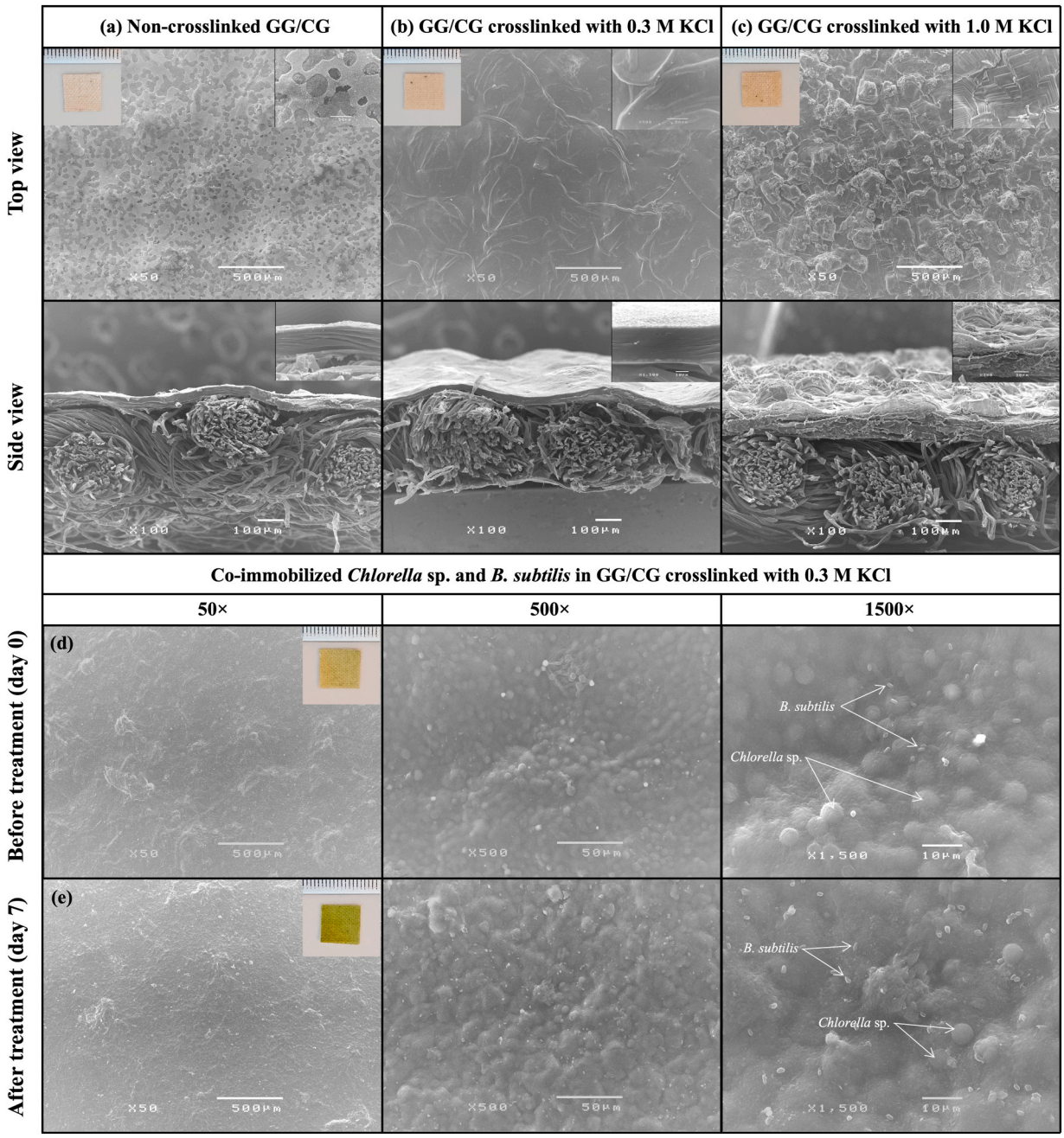

Fig. 5. SEM images of GG/CG hydrogels coated on cotton fabric under varying crosslinking conditions: (a) non-crosslinked, (b) crosslinked with 0.3 M KCl, and (c) crosslinked with 1.0 M KCl. SEM images of biofilter samples containing co-immobilized *Chlorella* sp. and *B. subtilis* in GG/CG hydrogels crosslinked with 0.3 M KCl: (d) before (day 0), and (e) after effluent treatment trials (day 7).

inverse relationship between KCl concentration in hydrogels and cell viability aligns with findings from recent studies examining the cytotoxic effects of ionic-crosslinked hydrogels. For example, Wood et al. (2025) demonstrated that increasing calcium chloride ($CaCl_2$) concentrations, crosslinking agent, resulted in a decline in cell viability suggesting that higher ionic concentrations could induce cytotoxicity within crosslinked hydrogels. This aligns with our results, where higher concentrations of KCl in the hydrogel led to a significant decrease in the viability of CS/BS co-culture. Both studies demonstrated that the presence of specific ions in hydrogels, whether KCl or $CaCl_2$, enhanced the crosslinking density and mechanical properties of the hydrogel matrix. However, this improvement came at the cost of cytotoxicity, as higher ionic concentrations impaired cell viability.

After solubility, water uptake, adhesion, and cytotoxicity tests were achieved for each hydrogel formulation, the decision matrix (Fig. 3c) was used to select the optimal hydrogel formulation for producing co-immobilized microalgal-bacterial biofilters for effluent treatment tests. The results showed that GG/CG crosslinked with KCl at a concentration of 0.3 M received the highest overall score because this KCl concentration was not too toxic to the cells and still had sufficient adhesion capacity, while also maintaining water absorption capacity and water solubility at levels that were not too high, making it stable enough to be used in effluent treatment trials.

3.2. *Effect of crosslinking on the stability of hydrogels*

Fig. 4a illustrates a three-stage schematic of the hydrogel crosslinking process and gelation mechanism (Wong, 2018). Initially, the GG

and CG polymers exist as individual, randomly coiled chains in solution (random coil stage). Upon the addition of a crosslinking agent like KCl, the negatively charged groups on polymer chains interact with K^+. This electrostatic interaction facilitates the formation of double-stranded helical structures between the polymer chains (double-stranded helix formation stage). Further aggregation of these helices occurs through additional inter- and intra-molecular interactions, forming a three-dimensional network (aggregation of helices). This intricate network structure physically traps the solvent molecules, resulting in hydrogel formation.

The gelation mechanism of a GG and CG mixture in the presence of K^+ results from a combination of ionic and hydrogen bonding interactions (Fig. 4b). The primary crosslinking mechanism, particularly in CG, involves ionic interactions between K^+ and the negatively charged sulfate ester groups ($-OSO_3^-$) located along the CG polymer backbone (Mirzaei et al., 2023; Rhein-Knudsen et al., 2015). These sulfate groups exhibit a affinity for K^+, forming stable ionic bonds (salt bridges) (Rhein-Knudsen et al., 2015). GG, a galactomannan polysaccharide, contains hydroxyl ($-OH$) groups that facilitate hydrogen bonding, thereby contributing to the network structure and stability of hydrogels (Wang et al., 2023). However, the primary crosslinking interactions occurred with the sulfate groups present in CG. Higher K^+ concentrations led to denser networks with increased ionic crosslinking, as evidenced by lower water uptake and reduced solubility, which indicates a more compact structure that restricts water diffusion into the hydrogel matrix. Conversely, lower K^+ concentrations resulted in weaker, more soluble hydrogels with enhanced water absorption, as indicated by water uptake and solubility tests.

The FTIR spectra of crosslinked GG/CG hydrogel with KCl are presented in Fig. 4c and summarized in Table 3 to identify the various functional groups and structural interaction present on them. The peak in the higher wavenumber region, around 3340 cm^{-1}, indicated the stretching vibration of hydroxyl groups (–OH) present in both GG and CG, while the band at 2914 cm^{-1} represented the C–H stretching vibration mode (Nandal et al., 2025). These hydroxyl group peaks might have been related to hydrogen bonding, which contributed to the overall structure of the hydrogel, or possibly to the residual moisture in the sample before analysis. The band around 1600-1700 cm^{-1} (C=O stretching) and the bands around 1420-1370 cm^{-1} (C–H bending) were characteristic of CC and GG (Lei et al., 2022) and showed minor intensity changes with KCl addition. Specifically, the bands around 1230 cm^{-1} (asymmetric stretching) and 1024 cm^{-1} (symmetric stretching) of the sulfate group ($–SO_3^-$) in CG (Markale et al., 2023; Nandal et al., 2025) showed peak intensity changes with increasing KCl concentration, which might have indicated the interaction between K^+ and sulfate groups. The variations in these band intensities observed with increasing KCl concentration further supported the formation of crosslinks within the hydrogel structure, involving both hydrogen bonding with hydroxyl groups and K^+ ionic interactions with sulfate groups.

The SEM images (Fig. 5a–c) illustrate the effects of increasing KCl concentration on the degree of crosslinking, morphology, physical structure, and porosity of GG/CG hydrogels coated on cotton fabric. In the absence of crosslinking (Fig. 5a), the GG/CG coating exhibits a loosely organized matrix characterized by irregular voids and a heterogeneous surface with high porosity, indicating the lack of a crosslinked polymeric network. The side view further reveals a discontinuous and thin polymer layer on the cotton substrate. This unstructured appearance is attributed to the absence of ionic interactions, resulting in a loosely entangled hydrogel matrix with limited mechanical integrity and a disordered morphology. Upon the introduction of 0.3 M KCl (Fig. 5b), the SEM images reveal a clear transition toward a more organized and cohesive physical structure. The top view displays a reduction in pore size and surface roughness, while the surface becomes smoother and more homogeneous. The side view reveals a denser and more uniformly distributed hydrogel layer covering the cotton surface. These morphological changes are attributed to moderate ionic crosslinking facilitated by K^+ ions, which bridge sulfate groups on carrageenan chains, forming a stable three-dimensional network and a tighter matrix (Markale et al., 2025). This partial crosslinking improves the structural integrity of the hydrogel, reducing pore size and number while maintaining some degree of flexibility and permeability. At the highest KCl concentration (1.0 M, Fig. 5c), the hydrogel exhibits a markedly compact structure with a higher crosslink density. The top view reveals a dense, very rough surface with minimal visible porosity; some microcracks or crystalline domains may be observed, likely due to drying-induced shrinkage in the highly crosslinked matrix (Markale et al., 2025). The side view shows a much thicker hydrogel layer that fully covers the cotton fabric. This indicates a high degree of ionic crosslinking, resulting in a tightly packed polymer network with greatly reduced porosity. Overall, increasing KCl concentration leads to a denser, less porous morphology. In other words, higher KCl levels promote the formation of more ionic bridges between polysaccharide chains, thereby enhancing crosslink density and compacting the hydrogel microstructure.

The SEM images (Fig. 5d and e) illustrate the surface morphology of biofilter samples containing co-immobilized CS and BS within a GG/CG hydrogel matrix crosslinked with 0.3 M KCl, coated onto cotton fabric. The images offer insights into microbial distribution, retention, and the role of the physical matrix during the effluent treatment trials. Before effluent treatment tests (Fig. 5d), the hydrogel matrix appears relatively continuous, suggesting uniform coating on the cotton substrate. At higher magnification (×1500), both CS and BS cells are visible and distinguishable, with CS appearing as spherical microalgae (~5 μm) and BS as smaller rod-shaped structures. The cells are well-distributed across the hydrogel surface, indicating effective co-immobilization within the crosslinked network. The suitable crosslink density and gel-like consistency of the GG/CG matrix at 0.3 M KCl provide a favorable environment for microbial entrapment, preventing cell detachment while maintaining cell retention and sufficient permeability for nutrient diffusion. After 7 days of effluent treatment trials (Fig. 5e), the hydrogel matrix appears rougher and more textured, likely due to microbial growth, metabolic activity, and interactions with components in the effluent. The number and distribution of microbial cells appear to increase, indicating active proliferation and colonization. This suggests that the hydrogel matrix successfully supported microbial viability and metabolic function during effluent exposure. Additionally, the denser surface texture may reflect the accumulation of bioproducts, adsorbed nutrients, or extracellular polymeric substances (EPS), which contribute to a more complex microenvironment (Caldwell et al., 2021; Janpum et al., 2022).

One important factor that can explain the efficiency of removing nutrients and organics is the rheological properties. Caldera-Villalobos et al. (2021) described composite collagen–guar gum hydrogels enhanced with metal–organic frameworks (MOFs), where the storage modulus of the hydrogel matrix increased dramatically (by 324.4 % with Mg-MOF and 116.8 % with Ca-MOF). This finding demonstrates that

Table 3
FTIR peaks and corresponding functional groups.

Wavenumber (cm^{-1})	Functional group	Description
3340	–OH (hydroxyl group)	Hydrogen bonding within hydrogel network or residual moisture
2914	C–H stretching	Backbone structure of GG and CG
1600–1700	C=O stretching	Structural feature of GG/CG matrix, minor intensity change observed with KCl addition
1420–1370	C–H bending	Backbone feature, slight variations with KCl addition
1230	$–SO_3^-$ (asymmetric stretch)	K^+ interaction with sulfate group, indicating crosslinking
1024	$–SO_3^-$ (symmetric stretch)	K^+ interaction with sulfate group, indicating crosslinking

added structural components, such as MOFs or cross-linkers, can enhance the stiffness of the polymer network, leading to increased elasticity that correlates with improved mechanical integrity and enables the hydrogel to better withstand shear forces and maintain its structure during treatment. In addition, Lei et al. (2022) studied hybrid gels with κ-CG or GG and observed that both storage (G′) and loss (G″) modulus generally rose as more polysaccharide was added. Specifically, G′ and G″ values increased with higher CG or GG content, indicating a stronger, denser gel network. Lei et al. (2022) also noted that very high GG content (above ~0.1 %) led to a slight drop in modulus, as entangled GG chains began to hinder the gel structure. These rheological results are consistent with our system, where increasing KCl crosslinker concentration similarly produces a denser GG/CG network and higher rigidity, as reflected in our solubility and swelling data, which in turn is expected to enhance pollutant removal in effluent. In summary, stronger gel rheology, characterized by higher modulus and rigidity and achieved through the incorporation of additional crosslinks or polymers, correlates with improved nutrient and organic removal. With further rheological analysis, it would entail flow properties and mechanical integrity of the biofilter, which would significantly help in scaling up for real-world applications including implementation with continuous or large-scale effluent treatment processes.

3.3. Nutrient removal efficiencies using the hydrogel-based biofilters

3.3.1. Ammonium removal

The NH_4^+ removal data demonstrated the effectiveness of the CS/BS system, with significantly enhanced removal achieved through co-culture compared to monocultures and the control (no added cells) within the hydrogel-based biofilters. Fig. 6a shows the percentage of NH_4^+ removal efficiency during 7 days of effluent treatment tests. In monocultures, CS showed a significantly higher NH_4^+ removal (87.23 ± 3.05 %) than BS (78.85 ± 3.97 %) after 7 days, (ANOVA: $F(1,4) = 8.40$, $p < 0.05$). This suggested that CS was the primary driver of NH_4^+ removal in this system, likely through direct assimilation into its biomass (Janpum et al., 2022). The lower removal by BS (78.85 ± 3.97 % on day 7) indicated its lower efficiency in NH_4^+ removal compared to CS. The co-culture biofilters showed higher NH_4^+ removal efficiencies than monocultures. The co-cultured biofilters showed significantly higher NH_4^+ removal efficiency than the monoculture and the control (no cells), (ANOVA: $F(5,12) = 336.22$, $p < 0.05$), especially the CS/BS ratio of 3:1 showed the highest removal efficiency (98.68 ± 1.32 % at day 7), demonstrating the synergistic effect of the co-culture. The 1:1 and 1:3 CS/BS ratios also improved removal compared to monocultures (95.15 ± 3.05 % and 88.55 ± 2.02 % at day 7, respectively), indicating that even with a lower proportion of CS, the co-culture enhances NH_4^+ removal. This synergistic effect was likely due to enhanced nutrient cycling and organic matter degradation, resulting from the interaction between CS (which provided oxygen) and BS (which degraded organic compounds, potentially making N more available), facilitating faster NH_4^+ uptake by the microalgae (Roy et al., 2023). The control condition (no cells) showed negligible NH_4^+ removal (18.50 ± 2.75 % at day 7), confirming that the observed removal in the other treatments resulted primarily from the biological activity of CS and/or BS. The significantly higher NH_4^+ removal efficiencies observed in the co-culture biofilters, compared to monocultures and the control, support the hypothesis that co-immobilization of CS and BS leads to enhanced nutrient removal through a synergistic interaction.

Our previous studies demonstrated that co-immobilized cultures of *Chlorella vulgaris* and BS removed 86.70 % of NH_4^+ and 99.30 % of PO_4^{3-} from synthetic municipal wastewater over seven days (Odibo et al., 2024). This performance was achieved using a 1:1 ratio of *C. vulgaris* and BS, indicating that even with a lower proportion of the microalga, the co-culture enhances NH_4^+ removal (Odibo et al., 2024). Guo et al. (2021) studied the immobilization of BS within a chitosan-sodium alginate composite carrier for ammonia (NH_3) removal from anaerobically digested swine wastewater, achieving a 96.50 % of NH_3-N removal efficiency with contributions from both adsorption and microbial action under optimized conditions. Furthermore, Nishi et al. (2022) investigated the co-cultivation of *Chlorella sorokiniana* and nitrifying bacteria under strong light conditions using a light-shielding hydrogel composed of alginate supplemented with carbon black. The results showed that the light-shielding hydrogel of co-culture significantly improved the nitrification efficiency, achieving a nitrification rate approximately 9 times higher than that of bacterial monoculture and exhibiting ammonia removal up to 74.0 %. This suggests that incorporating light-absorbing materials into immobilization matrices can effectively protect sensitive microbial communities from photoinhibition, thereby maintaining high N removal efficiencies under intense illumination. Compared to our study, which achieved a 98.68 % NH_4^+ removal efficiency at day 7 using a natural GG/CG hydrogel under moderate light conditions, Nishi et al. (2022)'s approach highlights the potential benefits of tailored hydrogel formulations for specific environmental challenges.

The NH_4^+ absorption rates are presented in Table 4. A general decline in the absorption rate was observed across all treatments from day 1 to day 7. This decrease was likely attributable to several interconnected factors such as the decreasing NH_4^+ concentration in the wastewater as treatment progressed, and potential nutrient limitation, where the available NH_4^+ was largely consumed (Sui et al., 2014). On first day, the co-culture biofilters demonstrated significantly higher NH_4^+ absorption rates than the monocultures, (ANOVA: $F(4,10) = 166.27$, $p < 0.05$), especially the CS/BS ratio of 3:1 exhibited the highest rate (1.92 ± 0.03 $mg{\cdot}day^{-1}{\cdot}g^{-1}_{biomass}$), followed by the 1:1 (1.82 ± 0.07 $mg{\cdot}day^{-1}{\cdot}g^{-1}_{biomass}$) and 1:3 (1.42 ± 0.06 $mg{\cdot}day^{-1}{\cdot}g^{-1}_{biomass}$) ratios. In contrast, the monocultures showed lower absorption rates: 1.32 ± 0.02 $mg{\cdot}day^{-1}{\cdot}g^{-1}_{biomass}$ for CS and 1.07 ± 0.04 $mg{\cdot}day^{-1}{\cdot}g^{-1}_{biomass}$ for BS. The observed rapid consumption of NH_4^+ in co-cultures, leading to a swift decline in uptake rates as NH_4^+ concentrations decrease, has been documented in various studies. For instance, Morán-Valencia et al. (2023) investigated N removal using an immobilized consortium of microalgae and nitrifying bacteria encapsulated in hybrid hydrogels composed of polyvinyl alcohol and sodium alginate. The study evaluated the performance of these hydrogels, both with and without the addition of activated carbon (AC), over 72 h period in treating synthetic wastewater. The hydrogels without AC could efficiently remove NH_4^+ (95.5 %) for 5 % biomass content. In contrast, the hydrogels with AC showed lower NH_4^+ removal efficiency (73.6 %), indicating that the presence of AC may inhibit the nitrification process. This suggests that the hybrid hydrogel matrix effectively supports the nitrification process, and that the inclusion of AC may not be necessary for removing potential inhibitors in such systems. The developed hydrogel facilitated NH_4^+ absorption through electrostatic interactions. It was composed of GG and CG, and its network was rich in negatively charged functional groups, such as hydroxyl and sulfate ions. These anionic sites attracted and bound positively charged NH_4^+ ions from wastewater via electrostatic interactions, effectively removing them from the solution (Cruz et al., 2018). This principle aligned with the findings of Cruz et al. (2018), whose studies on poly(acrylic acid)-based hydrogels demonstrated efficient NH_4^+ removal through similar ionic attractions.

In microalgae-bacteria co-cultures, N removal is achieved through a combination of assimilation by microalgae and nitrification by bacteria (Fig. 7a). Wastewater most typically contains inorganic N in the forms of ammonium-nitrogen (NH_4^+-N), nitrite-nitrogen (NO_2^--N), and nitrate-nitrogen (NO_3^--N) (Xu et al., 2024b). Microalgae play a vital role in assimilation, converting inorganic N into amino acids after transporting it into their cells. Before assimilation, enzymes like nitrate reductase and nitrite reductase transform all N forms into NH_4^+-N (Xu et al., 2024b). Subsequently, microalgae utilize the glutamine synthetase (GS) and glutamine oxoglutarate transaminase (GOGAT) cycle to convert NH_4^+-N into amino acids (Xu et al., 2024b). Bacteria, on the other hand, mainly contribute to N removal through nitrification, facilitated by the oxygen produced by microalgae (Janpum et al., 2022). Nitrification involves the

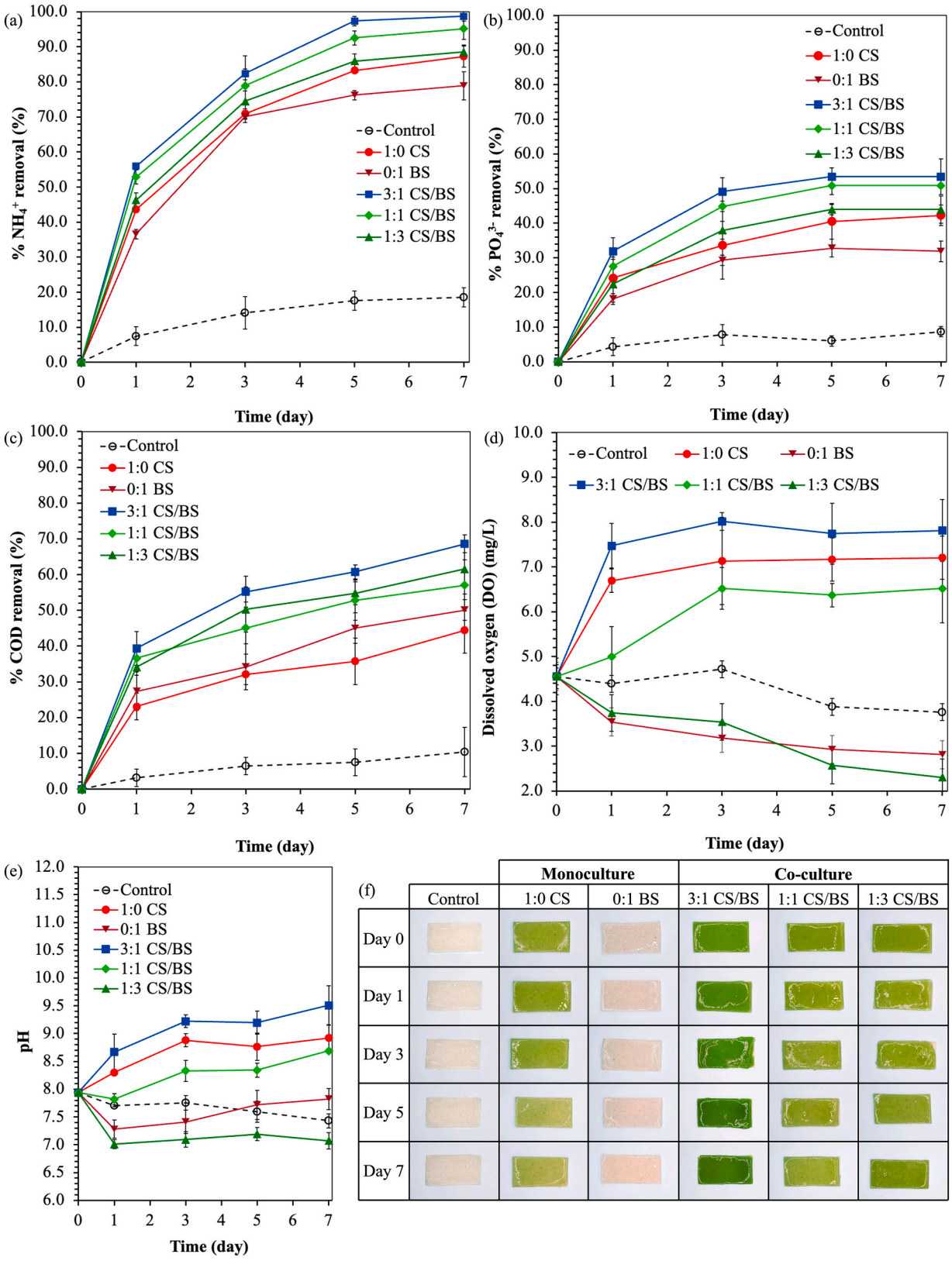

Fig. 6. The percentage removal efficiency of (a) NH_4^+, (b) PO_4^{3-}, and (c) COD, along with the variations in (d) DO, (e) pH in different CS/BS ratios within the hydrogel-based biofilters during effluent treatment, and (f) photographs of hydrogel-based biofilter samples after effluent treatment.

Table 4
Nutrient absorption rate of NH_4^+ and PO_4^{3-} using the hydrogel biofilters during effluent treatment, which differed significantly ($p < 0.05$, ANOVA, Tukey's post hoc test) and are denoted by *different capital letters*, columns for time points (day 1, 3, 5, and 7), and *lowercase letters*, rows for CS/BS ratios.

NH_4^+ absorption rate ($mg \cdot day^{-1} \cdot g^{-1}_{biomass}$)					
Time (day)	Monoculture 1:0 CS	0:1 BS	Co-culture 3:1_CS/BS	1:1_CS/BS	1:3_CS/BS
1	1.32 ± 0.02^{Aa}	1.07 ± 0.04^{Ab}	1.92 ± 0.03^{Ac}	1.82 ± 0.07^{Ac}	1.42 ± 0.06^{Aa}
3	0.72 ± 0.01^{Ba}	0.68 ± 0.01^{Ba}	0.94 ± 0.06^{Bb}	0.90 ± 0.06^{Bb}	0.76 ± 0.06^{Ba}
5	0.50 ± 0.01^{Ca}	0.44 ± 0.01^{Cb}	0.67 ± 0.01^{Cc}	0.64 ± 0.01^{Cd}	0.528 ± 0.01^{Ca}
7	0.38 ± 0.01^{Da}	0.33 ± 0.02^{Db}	0.48 ± 0.01^{Dc}	0.47 ± 0.02^{Dc}	0.389 ± 0.01^{Da}
PO_4^{3-} absorption rate ($mg \cdot day^{-1} \cdot g^{-1}_{biomass}$)					
Time (day)	Monoculture 1:0 CS	0:1 BS	Co-culture 3:1 CS/BS	1:1 CS/BS	1:3 CS/BS
1	37.28 ± 8.32^{Aac}	26.97 ± 2.22^{Aa}	55.96 ± 6.93^{Abd}	48.41 ± 4.54^{Acd}	35.21 ± 8.13^{Aac}
3	17.31 ± 5.04^{Ba}	14.56 ± 0.74^{Ba}	28.74 ± 2.31^{Bb}	26.22 ± 0.87^{Bbc}	19.86 ± 1.35^{Bac}
5	12.52 ± 1.60^{Ba}	9.76 ± 0.77^{Cb}	18.75 ± 0.91^{Cc}	17.85 ± 0.91^{Cc}	13.81 ± 0.47^{Ba}
7	9.32 ± 0.66^{Bac}	6.79 ± 0.63^{Ca}	13.40 ± 1.30^{Cb}	12.75 ± 0.65^{Cb}	9.87 ± 0.89^{Bc}

oxidation of NH_4^+-N to NH_2OH by ammonia monooxygenase (AMO) (Janpum et al., 2022). Next, hydroxylamine oxidase (HAO), oxidizes NH_2OH to NO_2^- (Janpum et al., 2022). Finally, NO_2^- is oxidized to NO_3^- by nitrite oxidoreductase (NXR) (Janpum et al., 2022). Additionally, bacteria also convert NH_4^+-N for amino acid synthesis, like microalgae, highlighting a shared pathway for N assimilation.

3.3.2. Phosphate removal

The PO_4^{3-} removal efficiency during seven days of effluent treatment is presented in Fig. 6b. The PO_4^{3-} removal data obtained from the hydrogel-immobilized biofilter system reveal a pattern consistent with the previously discussed NH_4^+ removal results, highlighting the synergistic effect of co-immobilizing CS and BS. The CS monoculture demonstrated a significantly higher PO_4^{3-} removal rate of 42.24 ± 2.99 %, in contrast to the BS monoculture, which had a removal rate of 31.90 ± 2.99 % after seven days, (ANOVA: $F(1,4) = 17.99$, $p < 0.05$). This suggests that CS played a key role in PO_4^{3-} uptake through assimilation, consistent with the finding that CS was also primarily responsible for NH_4^+ removal. Similar to NH_4^+ removal, PO_4^{3-} removal was significantly increased in the co-culture compared to single-culture systems and the control (no cells) after seven days, (ANOVA: $F(5,12) = 70.66$, $p < 0.05$). The co-cultures showed higher PO_4^{3-} removal efficiencies (53.45 ± 5.17 % for 3:1 ratio, 50.86 ± 2.59 % for 1:1 ratio, and 43.97 ± 3.95 % for 1:3 ratio at day 7), exceeding monocultures and suggesting a synergistic interaction between the two microorganisms (Bedane and Asfaw, 2023). After seven days of effluent treatment, visible differences in the hydrogel-based biofilters were observed, as shown in Fig. 6f. The biofilters containing co-immobilized CS and BS exhibited noticeable changes in coloration, which might have indicated microbial activity and pollutant adsorption. Additionally, the three-dimensional network of the GG/CG hydrogels likely contributes to this performance. The porous structure supports efficient transport of nutrients and gases (Yang et al., 2024), and the increased porosity of the hydrogels is known to enhance the diffusion of the substrate into the immobilized microbial communities (Song et al., 2023; Yang et al., 2024). Similarly, the crosslinking density of the hydrogels controls the pore size: a higher

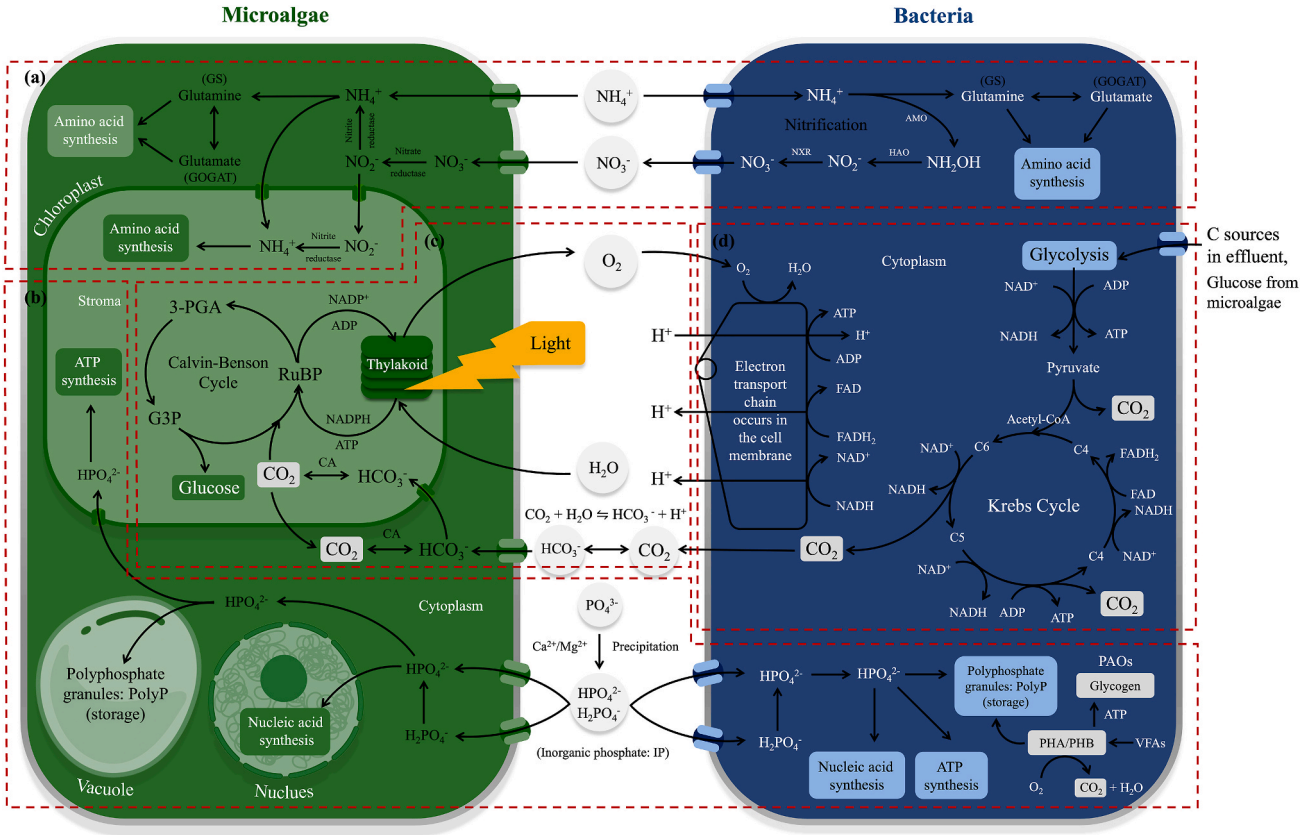

Fig. 7. Schematic representation of key nutrient pathways involved in effluent treatment using co-immobilized microalgae and bacteria, including (a) N removal via microalgal assimilation and bacterial nitrification, (b) P uptake and polyphosphate accumulation, (c) CO_2 consumption through microalgal photosynthesis, and (d) bacterial cellular respiration contributing to organic matter degradation (adapted from (Liu et al., 2024; Xu et al., 2024b; Zhang and Liu, 2021)).

degree of crosslinking creates a denser network with smaller pores (and lower permeability), whereas a lower degree leads to larger pores and higher permeability (Thang et al., 2023). The GG/CG matrix crosslinked with 0.3 M KCl in our study may appear to strike a balance between structural stability and porosity, providing a synergistic environment in which the 3:1 ratio of CS/BS co-cultures could efficiently access nutrients of NH_4^+ and PO_4^{3-}.

In comparison, recent research has shown different levels of P removal efficiency using different co-culture systems. In a study by Chang et al. (2023), a microalgae-bacteria consortium was investigated for the treatment of raw dairy manure wastewater using a novel two-stage process optimized over a six-day experiment. The first stage, conducted on day 1, involved anaerobic digestion to break down complex organic matter by bacteria. This was followed by a second stage on day 3, which employed an aerobic phase driven by a co-culture of microalgae and bacteria. The system achieved remarkable treatment efficiencies, including nearly 100 % removal of total phosphorus (TP) from an initial concentration of 71.1 $mg{\cdot}L^{-1}$. In addition to P, the study also reported high removal efficiencies for total nitrogen (TN) and COD, with TN reduced by up to 86.0 % and COD by up to 85.3 %. These results highlight the synergistic relationship between microalgae, which contribute to oxygen production and nutrient uptake, and bacteria, which facilitate the degradation of organic matter. In another investigation, Yang et al. (2023) developed an immobilized system using *Pseudomonas* sp. entrapped in a polyvinyl alcohol hydrogel matrix, enhanced with bentonite and lanthanum. This composite hydrogel system achieved an impressive 99.17 % of PO_4^{3-} removal efficiency from an initial concentration of 20.64 $mg{\cdot}L^{-1}$ (Yang et al., 2023). This removal efficiency is much higher than our system (53.45 % from an initial 386.67 $mg{\bullet}L^{-1}$), likely due to the lower initial PO_4^{3-} concentration in their study and the use of lanthanum and bentonite, which enhanced adsorption and co-precipitation processes, mechanisms absent in our biologically driven system. This system leveraged microbial-induced calcium precipitation, where the bacteria facilitated the co-precipitation of PO_4^{3-} with calcium ions, effectively removing it from the wastewater (Yang et al., 2023). Additionally, their study also reported high N removal efficiency, achieving 89.08 % of NH_4^+-N removal.

The PO_4^{3-} absorption rates ($mg{\cdot}day^{-1}{\cdot}g^{-1}$ biomass) from the hydrogel-based biofilter system, presented in Table 4, showed a pattern largely consistent with the NH_4^+ absorption rate results, further emphasizing the synergistic effect of co-immobilizing CS and BS. As observed with NH_4^+, PO_4^{3-} absorption rates decreased over time (day 1 to day 7) for all treatments. This decline was likely due to a combination of factors, including decreasing PO_4^{3-} concentrations in the wastewater and potential nutrient limitations (Peng et al., 2022). Similar to NH_4^+ uptake, the PO_4^{3-} absorption rates in the co-culture biofilters were significantly higher on first day compared to the monocultures and the control after seven days, (ANOVA: $F(4,10) = 29.19$, $p < 0.05$). The 3:1 CS/BS ratio demonstrated the highest initial rate (55.96 ± 6.93 $mg{\cdot}day^{-1}{\cdot}g^{-1}_{biomass}$), followed by the 1:1 (48.41 ± 4.54 $mg{\cdot}day^{-1}{\cdot}g^{-1}_{biomass}$) and 1:3 (35.21 ± 8.13 $mg{\cdot}day^{-1}{\cdot}g^{-1}_{biomass}$) ratios, suggesting synergistic effect of co-immobilization on initial PO_4^{3-} uptake. The monocultures showed considerably lower PO_4^{3-} absorption rates (37.28 ± 8.32 $mg{\cdot}day^{-1}{\cdot}g^{-1}_{biomass}$ for CS and 26.97 ± 2.22 $mg{\cdot}day^{-1}{\cdot}g^{-1}_{biomass}$ for BS on day 1).

P removal in microalgae-bacteria co-cultures relies on microalgae assimilation and P accumulation by polyphosphate-accumulating organisms (PAOs) (Fig. 7b). Orthophosphate (PO_4^{3-}), along with HPO_4^- and $H_2PO_4^-$, are the primary inorganic P forms in wastewater (Janpum et al., 2022; Qian et al., 2022). Microalgae absorb and utilize these P compounds, particularly HPO_4^- and $H_2PO_4^-$, during their growth. The removal process involves extracellular and intracellular stages. Extracellular processes include P precipitation with metal ions like calcium (Ca_2^+) or magnesium (Mg_2^+) and adsorption (Janpum et al., 2022). P plays a vital role in microalgal metabolism, being actively transported into cells and assimilated into biomass components like DNA, RNA, lipids, and ATP (Xu et al., 2024b). Intracellular processes, microalgae accumulate excess P as polyphosphate (PolyP) within vacuoles under high P concentrations, enabling them to cope with P-stressed conditions (Xu et al., 2024b). PAOs contribute to P removal by absorbing it under aerobic/anaerobic conditions to produce PolyP, which is then released anaerobically (Janpum et al., 2022; Xu et al., 2024b). PAOs oxidize polyhydroxyalkanoates (PHAs) and polyhydroxybutyrates (PHBs) to generate ATP for polyP formation and glycogen synthesis (Janpum et al., 2022; Xu et al., 2024b). Conversely, they can hydrolyze stored polyP to uptake volatile fatty acids (VFAs) and store them as PHAs/PHBs (Janpum et al., 2022; Xu et al., 2024b).

3.3.3. COD removal

This study investigated the COD removal efficiency of hydrogel-based biofilters system utilizing mono and co-cultures (Fig. 6c). The monoculture results showed that BS, 50.09 ± 2.84 % at day 7, achieved slightly higher COD removal than CS, 44.42 ± 6.44 % at day 7, throughout the treatment period. This suggested that bacterial metabolic activity played a more dominant role in COD reduction, primarily involving the breakdown of organic compounds, than microalgal assimilation (Roy et al., 2023). This contrasts with the PO_4^{3-} and NH_4^+ removal results, where CS was the primary driver. However, the co-culture showed significantly higher COD removal efficiencies compared to the monocultures and the control after seven days, (ANOVA: $F(5,12) = 37.45$, $p < 0.05$). Co-culture systems demonstrated better performance, with the 3:1 CS/BS ratio achieving the highest COD removal efficiency of 68.60 ± 2.52 % by day 7. The 1:3 and 1:1 CS/BS ratios also showed enhanced efficiencies, reaching 61.53 ± 6.98 % and 57.02 ± 7.15 %, respectively. This improvement can be attributed to the synergistic interactions between the microalgae and bacteria, where microalgae provides oxygen through photosynthesis, facilitating aerobic degradation by bacteria (Holmes et al., 2020). In contrast, control conditions without microbial inoculation showed minimal COD removal. In a study by Xu et al. (2025), two types of immobilized microalgal spheres were evaluated for treating simulated slaughtering wastewater. The first type utilized *Ankistrodesmus falcatus* immobilized within sodium alginate-silica hydrogel beads (SS-MS), while the second employed polyvinyl alcohol-sodium alginate hydrogel beads (PS-MS). The SS-MS configuration achieved notable removal efficiencies: 54.60 % for COD, 86.60 % for TP, and 62.08 % for NH_4^+-N. In contrast, the PS-MS system demonstrated higher TP removal at 90.31 % but significantly lower COD and NH_4^+-N removal rates of 9.30 % and 10.70 %, respectively. The superior COD removal observed with the SS-MS system is attributed to the enhanced mass transfer facilitated by the looser structure of the sodium alginate-silica beads, allowing better diffusion of organic substrates to the microalgal cells.

3.3.4. DO changes

The dissolved oxygen (DO) concentrations exhibit notable variations when comparing monocultures of CS and BS to their co-culture (Fig. 6d). In monocultures, CS demonstrated a significant increase in DO levels from 6.69 ± 0.26 $mg{\cdot}L^{-1}$ on day 1–7.20 ± 0.48 $mg{\cdot}L^{-1}$ by day 7, compared to the BS monoculture, (ANOVA: $F(1,4) = 194.09$, $p < 0.05$). This rise was attributed to the photosynthetic activity of microalgae, which produced oxygen as a byproduct, enriching the surrounding environment (Holmes et al., 2020). Conversely, BS cultures experienced a decline in DO concentrations, decreasing from 3.54 ± 0.10 $mg{\cdot}L^{-1}$ on day 1–2.81 ± 0.26 $mg{\cdot}L^{-1}$ by day 7. This reduction was likely due to the bacterial oxygen consumption during aerobic respiration processes (Holmes et al., 2020). In the co-culture, the 3:1 CS/BS ratio exhibited the highest dissolved oxygen (DO) levels, peaking at 8.02 ± 0.20 $mg{\cdot}L^{-1}$ on day 3, indicating the dominance of photosynthetic oxygen production. The 1:1 ratio showed a gradual increase in DO, reaching 6.52 ± 0.76 $mg{\cdot}L^{-1}$ by day 7. Meanwhile, the 1:3 CS/BS ratio started with a DO level of 3.74 ± 0.12 $mg{\cdot}L^{-1}$ on day 1, which declined to 3.54 ± 0.37 $mg{\cdot}L^{-1}$ by day 3 and further dropped to 2.30 ± 0.80 $mg{\cdot}L^{-1}$ by day 7. The higher proportion of BS in this co-culture likely led to increased oxygen

consumption, resulting in a continuous decline in DO concentrations. This phenomenon was evident in studies where co-cultures with a higher bacterial presence exhibited lower DO levels compared to those with a higher microalgal proportion. For instance, Sforza et al. (2018) reported that in co-cultures of microalgae and bacteria, the oxygen produced by microalgae was rapidly consumed by the bacterial population, leading to reduced DO levels in the medium.

3.3.5. pH changes

The pH changes over seven days of effluent treatment are illustrated in Fig. 6e. During the effluent treatment process using hydrogel-based biofilters of CS and BS, distinct pH dynamics were observed across different culture configurations. The initial pH was 7.94 ± 0.01. In the monoculture of CS, the pH increased gradually, reaching 8.30 ± 0.03 on day 1 and 8.92 ± 0.23 on day 7. Conversely, the BS monoculture

Table 5
The summary of various studies investigating immobilized hydrogel-based co-cultures or monocultures of microalgae and bacteria under different wastewater treatment conditions, with a focus on their efficiencies in removing COD, N, and P.

Microalgae	Bacteria	Immobilized condition	Cultivation mode	Wastewater type	Treatment time (days)	Removal efficiency (%) (final/initial concentration ($mg \cdot L^{-1}$))			Reference
						COD	N	P	
Chlorella sp.	*Bacillus subtilis*	Guar gum-carrageenan crosslink with KCl	Batch condition, Bottle-based glass, 25 °C, stir at 40 rpm, LED light 2000 lx, 12:12 dark-light cycle	Secondary effluent from vegetable oil industry	7	68.6 % (97.7/ 311.0)	NH_4^+: 98.7 % (0.04/ 3.6)	PO_4^{3-}: 53.5 % (179.8/ 386.7)	This study
Chlorella sorokiniana	Nitrifying bacteria	Sodium alginate-carbon black crosslink with $CaCl_2$	Batch condition, Crimp-top glass bottles, 25 °C, stir at 180 rpm, LED light 1600 $\mu mol \cdot m^{-2} \cdot s^{-1}$	Synthetic wastewater	1	N/A	NH_3: 74.0 % (13.2/ 50.8)	N/A	Nishi et al. (2022)
Chlorella vulgaris	Nitrifying bacteria	Polyvinyl alcohol-sodium alginate-activated carbon (AC)	Batch condition, Elenmeyer flasks, 27 °C, stir at 150 rpm, white light 160 $\mu mol \cdot m^{-2} \cdot s^{-1}$, 12:12 dark-light cycle	Synthetic wastewater	3	Failed (increased)	NH_4^+: 95.5 % (3.1/ 77.3) without AC 73.6 % (14.0/ 77.3) with AC	N/A	Morán-Valencia et al. (2023)
Chlorella sorokiniana	Acclimated mixed bacterial culture enriched from dairy manure	None (suspended)	Semi-batch condition, Serum bottle-based glass, 25 °C, stir at 150 rpm, white light 300 $\mu mol \cdot m^{-2} \cdot s^{-1}$, continuous illumination, aerated at 0.2 vvm with 2 % CO_2	Dairy manure wastewater	6 (3 days with bacteria, then 3 days with added microalgae)	85.3 % (488/ 3330)	TN: 86.0 % (20.4/ 145.4) NH_3-N: 99.6 % (0.4/ 99.3)	TP: 99.8 % (0.14/ 71.1)	Chang et al. (2023)
Chlorella vulgaris	*Bacillus subtilis*	Guar gum-carrageenan	Batch condition, Bottle-based glass, 25 °C, stir at 40 rpm, LED light 2000 lx, 12:12 dark-light cycle	Synthetic wastewater	7	N/A	NH_4^+: 86.7 % (8.9/ 67.1)	PO_4^{3-}: 99.3 % (0.2/ 29.9)	Odibo et al. (2024)
None	*Bacillus subtilis*	Sodium alginate-chitosan-acetic acid crosslink with $CaCl_2$	Batch condition, Beaker, 25 °C, stir at 200 rpm	Anaerobically digested swine wastewater	6	N/A	NH_3-N: 96.5 % (23.9/ 685.4)	N/A	Guo et al. (2021)
None	*Pseudomonas* sp.	Polyvinyl alcohol-bentonite-lanthanum	Continuous condition, Bioreactor (BR), 9 periods (HRT 6 h and C/N 6.0 at period 3)	Synthetic wastewater	20 (period 3)	N/A	NH_4^+-N: 89.1 % (3.4/ 31.5)	PO_4^{3-} -P: 99.2 % (0.2/ 20.6)	Yang et al. (2023)
Tetradesmus obliquus	None	Sodium alginate crosslink with $CaCl_2$	Batch condition, Elenmeyer flasks, 22 °C, white light fluorescent lamps 40 W, aerated at 1 $L \cdot min^{-1}$	Biodigested swine manure	10	62.0 % (144/383)	TN: 65.0 % (12.1/ 34.5)	TP: 99.0 % (1.6/ 311.4)	Aguiar et al. (2024)
Ankistrodesmus falcatus	None	Sodium alginate-silica crosslink with $CaCl_2$	Continuous condition, Photobioreactor (PBR), 25 °C, light 2000 lx, 12:12 dark-light cycle	Simulated slaughtering wastewater	2	54.6 % (534/ 1176)	NH_4^+-N: 62.1 % (11.1/ 29.3)	TP: 86.6 % (2.3/ 17.2)	Xu et al. (2025)
		Polyvinyl alcohol-sodium alginate crosslink with $CaCl_2$				9.3 % (82.3/ 1176)	NH_4^+-N: 10.8 % (26.1/ 29.3)	TP: 90.3 % (1.7/ 17.2)	

exhibited a slight decrease in pH to 7.28 ± 0.17 on day 1, followed by a gradual rise to 7.82 ± 0.19 by day 7. Among the co-cultures, the CS/BS ratio of 3:1 showed the most significant pH increase, reaching a peak of 9.51 ± 0.35 on day 7 compared to other conditions, (ANOVA: $F(5,12) = 63.82, p < 0.05$). The 1:1 CS/BS co-culture experienced a moderate pH increase, reaching 8.69 ± 0.04 by day 7, while the 1:3 CS/BS ratio maintained a relatively stable pH of around 7.07 ± 0.15 throughout the observation period. The control condition, which lacked microbial cells, showed a slight decrease in pH from 7.70 ± 0.02 on day 1 to 7.43 ± 0.13 on day 7.

The observed pH fluctuations can be attributed to the metabolic activities and interactions between the microalgae and bacteria within the biofilter system. The interplay between microalgal photosynthesis and bacterial respiration significantly influences the pH of the system (Fig. 7c and d). Microalgae perform photosynthesis (Fig. 7c) by consuming CO_2, releasing oxygen, and converting CO_2 into glucose through the Calvin-Benson cycle. This process can increase pH due to the reduction of dissolved CO_2 in the medium (Zhang and Liu, 2021). Additionally, microalgae absorb bicarbonate (HCO_3^-) ions from the environment during photosynthesis, transport them to the chloroplast, and convert them into CO_2 by carbonic anhydrase (CA), which can further raise the pH of wastewater (Zhang and Liu, 2021). When photosynthetic activity dominates, such as in co-cultures with a higher proportion of microalgae, the pH rises. This phenomenon explains the continuous pH rise in the CS monoculture and the more pronounced increase in the 3:1 CS/BS co-culture. In contrast, bacterial cellular respiration (Fig. 7d), primarily through glycolysis and the Krebs cycle, consumes O_2, produces CO_2, and releases H^+ from the electron transport system as a metabolic byproduct (Liu et al., 2024). The CO_2 released into the surrounding environment affected pH, accounting for the initial pH decrease observed in the BS monoculture and systems with a higher bacterial proportion.

A compilation of publications that focused on the nutrient removal efficiency of co-immobilized hydrogel-based microalgae and bacteria in various wastewater treatment systems was summarized in Table 5. Based on Table 5, the co-immobilized hydrogel-based system developed in this study showed potential as a "best-in-class" or at least a highly viable alternative approach for wastewater treatment. The biofilter with a 3:1 ratio of CS to BS achieved COD and nutrient removal efficiencies that outperformed monoculture, co-culture, and other systems based on the initial nutrient concentrations reported in previous studies. In addition, the crosslinked GG/CG hydrogel used in this study demonstrated optimized water absorption, low cell leakage, and low cytotoxicity, distinguishing it from other immobilization methods, such as alginate-based systems, which tended to have higher cell leakage or poorer durability. Thus, although it may not have been a “first-in-class” approach in all indicators, its combination of real wastewater applicability, balanced performance, and simple materials made the hydrogel a very attractive alternative to existing systems. However, limitations of this study include the relatively short treatment duration and the need to evaluate long-term stability, microbial community dynamics, and scalability in real-world settings. Future research should focus on optimizing the system for continuous operation, testing with diverse wastewater types, and assessing economic feasibility to fully establish its practical applicability and potential for widespread adoption.

4. Conclusions

This study successfully developed a hydrogel-based living biofilter utilizing co-immobilized CS and BS for nutrient removal from secondary industrial effluent, which is sufficiently stable and hydrophilic. The optimized hydrogel formulation, incorporating guar gum and carrageenan with 0.3 M KCl as a crosslinking agent, demonstrated enhanced stability, moderate water uptake, and high microbial adhesion while maintaining cell viability. The co-culture biofilter of the 3:1 CS/BS mixing ratio exhibited a synergistic effect, significantly improving NH_4^+ (98.68 %), PO_4^{3-} (53.45 %), and COD (68.60 %) removal efficiencies compared to monocultures. The interaction between microalgae and bacteria facilitated nutrient uptake, organic matter degradation, and improved effluent treatment performance. The findings highlight the potential of hydrogel-based living biofilters as an effective and sustainable approach for wastewater treatment, promoting resource recovery while mitigating environmental pollution. Further research should focus on scaling up this system and assessing its long-term operational efficiency under real-world conditions.

CRediT authorship contribution statement

Chalampol Janpum: Writing – original draft, Visualization, Project administration, Methodology, Investigation, Data curation, Conceptualization. **Jagroop Pandhal:** Writing – review & editing, Validation, Supervision, Resources, Investigation, Formal analysis. **Nuttapon Pombubpa:** Writing – review & editing, Validation, Supervision, Resources, Methodology, Investigation, Formal analysis, Conceptualization. **Tanakit Komkhum:** Writing – review & editing, Visualization, Methodology, Data curation. **Chonnikarn Sirichan:** Writing – review & editing, Resources, Investigation. **Piyakorn Srichuen:** Writing – review & editing, Resources, Investigation. **Pichaya In-na:** Writing – review & editing, Validation, Supervision, Resources, Project administration, Methodology, Investigation, Funding acquisition, Conceptualization.

Declaration of competing interest

The authors declare that they have no known competing financial interests or personal relationships that could have appeared to influence the work reported in this paper.

Acknowledgments

This research project is supported by the Second Century Fund (C2F), Chulalongkorn University and grants for the development of new faculty staff (DNS 67_004_23_004_2), Ratchadaphiseksomphot Endowment Fund, Chulalongkorn University.

Data availability

Data will be made available on request.

References

Abdel-Raouf, M., 2019. Guar gum based hydrogels for sustained water release applications in agriculture, a review. Curr Res Biopolymers 2, 111. https://doi.org/10.29011/CRBP-111.000011.

Aboelkhir, D.M., Sayed, A., Eldondaity, L.S., Joseph, V., Amin, A., Mahmoud, G.A., 2024. Multiwalled carbon nanotubes@pectin/κ-carrageenan-based nanocomposite biohydrogel prepared by gamma irradiation for efficient methylene blue dye sequestration. J. Appl. Polym. Sci. 141 (22), e55452. https://doi.org/10.1002/app.55452.

Adhithya, S., Nithya, K., Satish, A., Kumar, V., 2025. Uncovering the feasibility of using live Chlorella microbiomes in domestic and industrial wastewater treatment: insights into monoculture and synergistic mixed co-cultured system. J. Ind. Eng. Chem. https://doi.org/10.1016/j.jiec.2025.02.006.

Afzaal, M., Nawaz, R., Hussain, S., Nadeem, M., Irshad, M.A., Irfan, A., Mannan, H.A., Al-Mutairi, A.A., Islam, A., Al-Hussain, S.A., 2024. Removal of oxytetracycline from pharmaceutical wastewater using kappa carrageenan hydrogel. Sci. Rep. 14 (1), 19687. https://doi.org/10.1038/s41598-024-69989-x.

Aguiar, Severo I., Azevedo, O.G.d.A., da Silva, P.A.S., Jacob-Furlan, B., Mariano, A.B., Ordonez, J.C., Vargas, J.V.C., 2024. Wastewater treatment process using immobilized microalgae. Water Sci. Technol. 90 (4), 1306–1320. https://doi.org/10.2166/wst.2024.283.

Bedane, D.T., Asfaw, S.L., 2023. Microalgae and co-culture for polishing pollutants of anaerobically treated agro-processing industry wastewater: the case of slaughterhouse. Bioresour. Bioprocess. 10 (1), 81. https://doi.org/10.1186/s40643-023-00699-4.

Bouabidi, Z.B., El-Naas, M.H., Zhang, Z., 2019. Immobilization of microbial cells for the biotreatment of wastewater: a review. Environ. Chem. Lett. 17, 241–257. https://doi.org/10.1007/s10311-018-0795-7.

Caldera-Villalobos, M., Cabrera-Munguía, D.A., Becerra-Rodríguez, J.J., Claudio-Rizo, J. A., 2022. Tailoring biocompatibility of composite scaffolds of collagen/guar gum with metal–organic frameworks. RSC Adv. 12 (6), 3672–3686. https://doi.org/10.1039/D1RA08824F.

Caldera-Villalobos, M., Cabrera-Munguía, D.A., Flores-Guía, T.E., Viramontes-Gamboa, G., Vargas-Correa, J.A., Cano-Salazar, L.F., Claudio-Rizo, J.A., 2021. Removal of water pollutants using composite hydrogels comprised of collagen, guar gum, and metal-organic frameworks. J. Polym. Res. 28 (10), 395. https://doi.org/10.1007/s10965-021-02767-9.

Caldwell, G.S., In-na, P., Hart, R., Sharp, E., Stefanova, A., Pickersgill, M., Walker, M., Unthank, M., Perry, J., Lee, J.G., 2021. Immobilising microalgae and cyanobacteria as biocomposites: new opportunities to intensify algae biotechnology and bioprocessing. Energies 14 (9), 2566. https://doi.org/10.3390/en14092566.

Caliari, S.R., Burdick, J.A., 2016. A practical guide to hydrogels for cell culture. Nat. Methods 13 (5), 405–414. https://doi.org/10.1038/nmeth.3839.

Chang, Y.L., Nagarajan, D., Chen, J.H., Chen, C.Y., Wu, Y.J., Whang, L.M., Lee, D.J., Chang, J.S., 2023. Microalgae-bacteria consortia for the treatment of raw dairy manure wastewater using a novel two-stage process: process optimization and bacterial community analysis. Chem. Eng. J. 473, 145388. https://doi.org/10.1016/j.cej.2023.145388.

Croitoru, C., Roata, I.C., Pascu, A., Stanciu, E.M., 2020. Diffusion and controlled release in physically crosslinked poly (vinyl alcohol)/iota-carrageenan hydrogel blends. Polym 12 (7), 1544. https://doi.org/10.3390/polym12071544.

Cruz, H., Luckman, P., Seviour, T., Verstraete, W., Laycock, B., Pikaar, I., 2018. Rapid removal of ammonium from domestic wastewater using polymer hydrogels. Sci. Rep. 8 (1), 2912. https://doi.org/10.1038/s41598-018-21204-4.

Guan, X., Avci, Adali M., Alarçin, E., Cheng, H., Kashaf, S.S., Li, Y., Chawla, A., Jang, H. L., Khademhosseini, A., 2017. Development of hydrogels for regenerative engineering. Biotechnol. J. 12 (5), 1600394. https://doi.org/10.1002/biot.201600394.

Guo, J., Chen, C., Chen, W., Jiang, J., Chen, B., Zheng, F., 2021. Effective immobilization of *Bacillus subtilis* in chitosan-sodium alginate composite carrier for ammonia removal from anaerobically digested swine wastewater. Chemosphere 284, 131266. https://doi.org/10.1016/j.chemosphere.2021.131266.

Hartal, O., Khattabi Rifi, S., Chatoui, M., Haddaji, C., Madinzi, A., Pala, A., Souabi, S., 2024. Combined natural flotation and chemical precipitation for the treatment of vegetable oil refinery wastewater. Int. J. Environ. Sci. Technol. 21 (10), 7295–7306. https://doi.org/10.1007/s13762-024-05470-6.

Holmes, B., Paddock, M.B., VanderGheynst, J.S., Higgins, B.T., 2020. Algal photosynthetic aeration increases the capacity of bacteria to degrade organics in wastewater. Biotechnol. Bioeng. 117 (1), 62–72. https://doi.org/10.1002/bit.27172.

In-na, P., Umar, A.A., Wallace, A.D., Flickinger, M.C., Caldwell, G.S., Lee, J.G., 2020. Loofah-based microalgae and cyanobacteria biocomposites for intensifying carbon dioxide capture. J. CO2 Util. 42, 101348. https://doi.org/10.1016/j.jcou.2020.101348.

Janpum, C., Pombubpa, N., Monshupanee, T., Incharoensakdi, A., In-na, P., 2022. Advancement on mixed microalgal-bacterial cultivation systems for nitrogen and phosphorus recoveries from wastewater to promote sustainable bioeconomy. J. Biotechnol. 360, 198–210. https://doi.org/10.1016/j.jbiotec.2022.11.008.

Ji, F., Shang, P., Lai, Y., Wang, J., Zhang, G., Lin, D., Xu, J., Cai, D., Qin, Z., 2023. Fully physically crosslinked conductive hydrogel with ultrastretchability, transparency, and self-healing properties for strain sensors. Materials 16 (19), 6491. https://doi.org/10.3390/ma16196491.

Komkhum, T., Sema, T., Rehman, Z.U., In-na, P., 2025. Carbon dioxide removal from triethanolamine solution using living microalgae-loofah biocomposites. Sci. Rep. 15 (1), 7247. https://doi.org/10.1038/s41598-025-90855-x.

Kosky, P., Balmer, R., Keat, W., Wise, G., 2021. Chapter 25 - design step 3: evaluation of alternatives and selection of a concept. In: Kosky, P., Balmer, R., Keat, W., Wise, G. (Eds.), Exploring Engineering. Academic Press, pp. 523–539. https://doi.org/10.1016/B978-0-12-815073-3.00025-9.

Lei, Y.C., Zhao, X., Li, D., Wang, L.J., Wang, Y., 2022. Effects of κ-carrageenan and guar gum on the rheological properties and microstructure of phycocyanin gel. Foods 11 (5), 734. https://doi.org/10.3390/foods11050734.

Li, K., Liu, Q., Fang, F., Luo, R., Lu, Q., Zhou, W., Huo, S., Cheng, P., Liu, J., Addy, M., 2019. Microalgae-based wastewater treatment for nutrients recovery: a review. Bioresour. Technol. 291, 121934. https://doi.org/10.1016/j.biortech.2019.121934.

Li, L., Chai, W., Sun, C., Huang, L., Sheng, T., Song, Z., Ma, F., 2024. Role of microalgae-bacterial consortium in wastewater treatment: a review. J. Environ. Manag. 360, 121226. https://doi.org/10.1016/j.jenvman.2024.121226.

Liu, Y., Li, T., Yang, C., Deng, H., 2024. Chapter 10 - bacterial energy metabolism. In: Tang, Y.W., Hindiyeh, M.Y., Liu, D., Sails, A., Spearman, P., Zhang, J.R. (Eds.), Molecular Medical Microbiology. Academic Press, pp. 177–200. https://doi.org/10.1016/B978-0-12-818619-0.00155-6.

Lopez Martinez, E.E., Claudio Rizo, J.A., Caldera, Villalobos M., Becerra Rodriguez, J.J., Cabrera Munguia, D.A., Cano Salazar, L.F., Betancourt, Galindo R., 2022. Hydrogels for biomedicine based on semi-interpenetrating polymeric networks of collagen/guar gum: synthesis and physicochemical characterization. Macromol. Res. 30 (6), 375–383. https://doi.org/10.1007/s13233-022-0047-3.

Lopéz Martínez, E.E., Claudio, Rizo J.A., Caldera, Villalobos M., Becerra Rodríguez, J.J., Cabrera Munguía, D.A., Cano Salazar, L.F., Betancourt, Galindo R., 2022. Hydrogels for biomedicine based on semi-interpenetrating polymeric networks of collagen/guar gum: applications in biomedical field and biocompatibility. Macromol. Res. 30 (6), 384–390. https://doi.org/10.1007/s13233-022-0048-2.

Markale, A., Mateti, T., Likhith, K., Bhatt, S.S., Rajesh, K., Managuli, V., Nune, M., Raval, R., Kumar, P., Thakur, G., 2023. Fostering K-carrageenan hydrogels with the power of natural crosslinkers: a comparison between tender coconut water and potassium chloride for antibacterial therapy. ChemRxiv. https://doi.org/10.26434/chemrxiv-2023-q7st6.

Markale, A., Mateti, T., Likhith, K., Bhatt, S.S., Rajesh, K., Managuli, V., Nune, M., Raval, R., Kumar, P., Thakur, G., 2025. Fostering kappa (κ)-carrageenan hydrogels with the power of a natural crosslinker: a comparison between tender coconut water and potassium chloride (KCl) for therapeutic applications. 3 Biotech 15 (4), 1–13. https://doi.org/10.1007/s13205-025-04254-0.

Mirzaei, A., Esmkhani, M., Zallaghi, M., Nezafat, Z., Javanshir, S., 2023. Biomedical and environmental applications of carrageenan-based hydrogels: a review. J. Polym. Environ. 31 (5), 1679–1705. https://doi.org/10.1007/s10924-022-02726-5.

Morán-Valencia, M., Nishi, K., Akizuki, S., Ida, J., Cuevas-Rodríguez, G., Cervantes-Avilés, P., 2023. Nitrogen removal from wastewater by an immobilized consortium of microalgae–bacteria in hybrid hydrogels. Water Sci. Technol. 87 (3), 527–538. https://doi.org/10.2166/wst.2023.001.

Nagabalaji, V., Maharaja, P., Nishanthi, R., Sathish, G., Suthanthararajan, R., Srinivasan, S.V., 2023. Effect of co-culturing bacteria and microalgae and influence of inoculum ratio during the biological treatment of tannery wastewater. J. Environ. Manag. 341, 118008. https://doi.org/10.1016/j.jenvman.2023.118008.

Nandal, K., Vaid, V., Saini, P., Sharma, R.K., Joshi, V., Jindal, R., Mittal, H., 2025. Synthesis and characterization of κ-carrageenan and guar gum-based hydrogels for controlled release fertilizers: optimization, release kinetics, and agricultural impact. Ind. Crops Prod. 225, 120587. https://doi.org/10.1016/j.indcrop.2025.120587.

Nasution, H., Harahap, H., Dalimunthe, N.F., Ginting, M.H.S., Jaafar, M., Tan, O.O., Aruan, H.K., Herfananda, A.L., 2022. Hydrogel and effects of crosslinking agent on cellulose-based hydrogels: a review. Gels 8 (9), 568. https://doi.org/10.3390/gels8090568.

Nicodemus, G.D., Bryant, S.J., 2008. Cell encapsulation in biodegradable hydrogels for tissue engineering applications. Tissue Eng., Part B 14 (2), 149–165. https://doi.org/10.1089/ten.teb.2007.0332.

Nishi, K., Akizuki, S., Toda, T., Matsuyama, T., Ida, J., 2022. Advanced light-tolerant microalgae-nitrifying bacteria consortia for stable ammonia removal under strong light irradiation using light-shielding hydrogel. Chemosphere 297, 134252. https://doi.org/10.1016/j.chemosphere.2022.134252.

Odibo, A., Janpum, C., Pombubpa, N., Monshupanee, T., Incharoensakdi, A., Rehman, Z. U., In-na, P., 2024. Microalgal-bacterial immobilized co-culture as living biofilters for nutrient recovery from synthetic wastewater and their potential as biofertilizers. Bioresour. Technol. 398, 130509. https://doi.org/10.1016/j.biortech.2024.130509.

Oladimeji, T., Oyedemi, M., Emetere, M., Agboola, O., Adeoye, J., Odunlami, O., 2024. Review on the impact of heavy metals from industrial wastewater effluent and removal technologies. Heliyon 10 (23), e40370. https://doi.org/10.1016/j.heliyon.2024.e40370.

Peng, Z., Wang, J., Niu, N., Liu, A., Niu, Y., Qin, J., Liu, M., Li, Y., 2022. The effect of PO_4^{3-}-P concentration on sludge settleability and nutrients removal performance. Water Sci. Technol. 86 (5), 1108–1121. https://doi.org/10.2166/wst.2022.248.

Princen, K., Marien, N., Guedens, W., Graulus, G.J., Adriaensens, P., 2023. Hydrogels with reversible crosslinks for improved localised stem cell retention: a review. Chembiochem 24 (20), e202300149. https://doi.org/10.1002/cbic.202300149.

Qian, J., Chen, F., Zhou, W., 2022. Chapter Five - advancements of application of microalgae biotechnology in the aquaculture water quality control. In: Li, Y., Zhou, Y. (Eds.), Advances in Bioenergy, vol. 7. Elsevier, pp. 167–210. https://doi.org/10.1016/bs.aibe.2022.05.002.

Rahman, S., Konwar, A., Majumdar, G., Chowdhury, D., 2021. Guar gum-chitosan composite film as excellent material for packaging application. Carbohydr. Polym. Technol. Appl. 2, 100158. https://doi.org/10.1016/j.carpta.2021.100158.

Rando, G., Scalone, E., Sfameni, S., Plutino, M.R., 2024. Functional bio-based polymeric hydrogels for wastewater treatment: from remediation to sensing applications. Gels 10 (8), 498. https://doi.org/10.3390/gels10080498.

Rhein-Knudsen, N., Ale, M.T., Meyer, A.S., 2015. Seaweed hydrocolloid production: an update on enzyme assisted extraction and modification technologies. Mar. Drugs 13 (6), 3340–3359. https://doi.org/10.3390/md13063340.

Roy, C., Sen, P., Vurimindi, H., 2023. Kinetic modeling and experiments on removal of COD/nutrients from dairy effluent using chlorella and co-culture. Bioproc. Biosyst. Eng. 46 (8), 1099–1110. https://doi.org/10.1007/s00449-023-02894-1.

Sayed, A., Mahmoud, A.F., Aly, A.M., Emad, K., Mahmoud, G.A., 2023. Design of carrageenan based nanocarrier as a drug nanocarrier for tumor targeting: radiolabeling and biodistribution. J. Drug Deliv. Sci. Technol. 85, 104573. https://doi.org/10.1016/j.jddst.2023.104573.

Sforza, E., Pastore, M., Spagni, A., Bertucco, A., 2018. Microalgae-bacteria gas exchange in wastewater: how mixotrophy may reduce the oxygen supply for bacteria. Environ. Sci. Pollut. Res. 25, 28004–28014. https://doi.org/10.1007/s11356-018-2834-0.

Shamshad, J., Rehman, R.U., 2025. Innovative approaches to sustainable wastewater treatment: a comprehensive exploration of conventional and emerging technologies. Env. Sci. Adv. 4 (2), 189–222. https://doi.org/10.1039/D4VA00136B.

Sial, A., Zhang, B., Zhang, A., Liu, K., Imtiaz, S.A., Yashir, N., 2021. Microalgal–bacterial synergistic interactions and their potential influence in wastewater treatment: a review. Bioenergy Res. 14, 723–738. https://doi.org/10.1007/s12155-020-10213-9.

Solbu, A.A., Caballero, D., Damigos, S., Kundu, S.C., Reis, R.L., Halaas, Ø., Chahal, A.S., Strand, B.L., 2023. Assessing cell migration in hydrogels: an overview of relevant materials and methods. Mater. Today Bio 18, 100537. https://doi.org/10.1016/j.mtbio.2022.100537.

Song, M., Yuan, M., Jeong, S., Bae, H., 2023. Thickness of hydrogel for nitrifying biomass entrapment determines the free ammonia susceptibility differently in batch and continuous modes. Sci. Rep. 13 (1), 9353. https://doi.org/10.1038/s41598-023-36507-4.

Srimongkol, P., Sangtanoo, P., Songserm, P., Watsuntorn, W., Karnchanatat, A., 2022. Microalgae-based wastewater treatment for developing economic and environmental

sustainability: current status and future prospects. Front. Bioeng. Biotechnol. 10, 904046. https://doi.org/10.3389/fbioe.2022.904046.

Sui, Q., Liu, C., Dong, H., Zhu, Z., 2014. Effect of ammonium nitrogen concentration on the ammonia-oxidizing bacteria community in a membrane bioreactor for the treatment of anaerobically digested swine wastewater. J. Biosci. Bioeng. 118 (3), 277–283. https://doi.org/10.1016/j.jbiosc.2014.02.017.

Thang, N.H., Chien, T.B., Cuong, D.X., 2023. Polymer-based hydrogels applied in drug delivery: an overview. Gels 9 (7), 523. https://doi.org/10.3390/gels9070523.

Trejo, A., De-Bashan, L.E., Hartmann, A., Hernandez, J.P., Rothballer, M., Schmid, M., Bashan, Y., 2012. Recycling waste debris of immobilized microalgae and plant growth-promoting bacteria from wastewater treatment as a resource to improve fertility of eroded desert soil. Environ. Exp. Bot. 75, 65–73. https://doi.org/10.1016/j.envexpbot.2011.08.007.

Van Tran, V., Park, D., Lee, Y.C., 2018. Hydrogel applications for adsorption of contaminants in water and wastewater treatment. Environ. Sci. Pollut. Res. 25, 24569–24599. https://doi.org/10.1007/s11356-018-2605-y.

Wang, Y., Yang, M., Zhao, Z., 2023. Facile fabrication of self-healing, injectable and antimicrobial cationic guar gum hydrogel dressings driven by hydrogen bonds. Carbohydr. Polym. 310, 120723. https://doi.org/10.1016/j.carbpol.2023.120723.

Wang, X., Jiang, J., Gao, W., 2022. Reviewing textile wastewater produced by industries: characteristics, environmental impacts, and treatment strategies. Water Sci. Technol. 85 (7), 2076–2096. https://doi.org/10.2166/wst.2022.088.

Wang, Z., Li, Z., Gao, C., Jiang, Z., Huang, S., Li, X., Yang, H., 2025. *Bacillus subtilis* as an excellent microbial treatment agent for environmental pollution: a review. Biotechnol. J. 20 (4), e70026. https://doi.org/10.1002/biot.70026.

Wong, D.W.S., 2018. Carbohydrates, Mechanism and Theory in Food Chemistry. Springer International Publishing, Cham, pp. 123–168. https://doi.org/10.1007/978-3-319-50766-8_3.

Wood, N., Doria, E.I., Rahman, T.T., Li, W., Pei, Z., Qin, H., 2025. Effects of calcium chloride crosslinking colution concentration on the long-term cell viability of 16HBE14o- human bronchial cells embedded in alginate-based hydrogels. Biomimetics 10 (1), 40. https://doi.org/10.3390/biomimetics10010040.

Wu, Y., Joseph, S., Aluru, N., 2009. Effect of cross-linking on the diffusion of water, ions, and small molecules in hydrogels. J. Phys. Chem. B 113 (11), 3512–3520. https://doi.org/10.1021/jp808145x.

Xu, H., Liu, C., Wang, A., Yue, B., Lin, T., Ding, M., 2024a. Microalgae treatment of food processing wastewater for simultaneous biomass resource recycling and water reuse. J. Environ. Manag. 369, 122394. https://doi.org/10.1016/j.jenvman.2024.122394.

Xu, S., Li, Z., Yu, S., Chen, Z., Xu, J., Qiu, S., Ge, S., 2024b. Microalgal–bacteria biofilm in wastewater treatment: advantages, principles, and establishment. Water 16 (18), 2561. https://doi.org/10.3390/w16182561.

Xu, W., Zhang, X., Zhang, G., Zhang, X., 2025. Removal of TP, COD, and NH_4^+-N in simulated slaughtering wastewater by two kinds of immobilized microalgal spheres. Water 17 (2), 179. https://doi.org/10.3390/w17020179.

Yang, G., Zhang, J., Abdullah, R., Cheah, W.Y., Zhao, D., Ling, T.C., 2024. Comprehensive advancements in hydrogel, and its application in microalgae cultivation and wastewater treatment. J. Microbiol. Biotechnol. 35, e2407038. https://doi.org/10.4014/jmb.2407.07038.

Yang, W., Xu, L., Su, J., Wang, Z., Zhang, L., 2023. Simultaneous removal of phosphate, calcium, and ammonia nitrogen in a hydrogel immobilized reactor with bentonite/lanthanum/PVA based on microbial induced calcium precipitation. Chemosphere 326, 138460. https://doi.org/10.1016/j.chemosphere.2023.138460.

Yousry, R., Sayed, A., Behalo, M.S., Abdel Raouf, M.E., Feteha, A., 2025. Tailoring of carboxymethyl guar gum hydrogels via gamma irradiation for remarkable removal of cationic and anionic dyes from simulated solutions. Int. J. Biol. Macromol. 284, 137867. https://doi.org/10.1016/j.ijbiomac.2024.137867.

Yusuf, R.O., Noor, Z.Z., Hassan, M.A.A., Agarry, S.E., Solomon, B.O., 2013. A comparison of the efficacy of two strains of *Bacillus subtilis* and *Pseudomonas fragii* in the treatment of tannery wastewater. Desalination Water Treat. 51 (16), 3189–3195. https://doi.org/10.1080/19443994.2012.751155.

Zhang, S., Liu, Z., 2021. Advances in the biological fixation of carbon dioxide by microalgae. J. Chem. Technol. Biotechnol. 96 (6), 1475–1495. https://doi.org/10.1002/jctb.6714.